Complexity-Sensitive Complementarity in Non-Isometric Holographic Codes

Adam R. Cagle
Independent researcher, Vancouver, WA
[email]

with Claude (Anthropic) as computational collaborator

April 24, 2026

Abstract

We prove that the expected entropic disagreement between two observers in the Akers–Engelhardt–Harlow–Penington–Vardhan (AEHPV) non-isometric holographic code, with both observers included via the Harlow–Usatyuk–Zhao (HUZ) cloning rule, depends non-trivially on the complexity of the bulk state. For product bulk states, the disagreement falls off as $d_B^{-1/2}$ with leading-order prefactor $\sqrt{4(\pi^2/3-3)/\pi} \approx 0.608$. For maximally-entangled (Haar) bulk states, it falls off as $d_B^{-3/2}$ with leading-order prefactor $\sqrt{2/\pi}/d_M \approx 0.1995/d_M$. Both asymptotic forms are derived rigorously from a single structural identity: the Haar-V average of each observer's reduced state equals the diagonal of the bulk marginal in a particular basis, with off-diagonal errors suppressed as $O(1/d^2)$. The integer exponent gap $\alpha_P - \alpha_H = 1$ reflects one power of d_B separating Dirichlet amplitude fluctuations (simple state) from Dirichlet eigenvalue fluctuations (complex state). All analytic predictions are verified against Monte Carlo simulation of the full HUZ+V pipeline at nine values of d_B, and against out-of-sample tests at d_B and d values not used in any calibration, at sub-2σ precision throughout. The result refines observer complementarity at the entropy level: state-class sensitivity at the entropy level is genuine, while the inner-product-level HUZ bound of $1/d_{\mathrm{Ob}}$ remains state-independent.

Contents

1 Introduction

1.1 Observer complementarity in non-isometric codes

In recent work, observer-dependent entropies have emerged as a central diagnostic of bulk reconstruction in non-isometric holographic codes. The essential tension is that different observer-inclusion rules — each motivated by different physical considerations and each a natural construction — give rise to different von Neumann entropies on the same bulk state. This disagreement is the quantitative content of *observer complementarity*: a bulk state has multiple coexisting entropic interpretations, and the gap between them is a feature, not a bug, of the non-isometric-code framework.

Two influential lines of work have crystallized specific versions of this picture. First, Akers, Engelhardt, Harlow, Penington, and Vardhan (AEHPV) [1] established the non-isometric-code framework itself: a random code $V : \mathcal{H}_{\text{eff}} \to \mathcal{H}_{\text{fund}}$ with $d_{\text{eff}} > d_{\text{fund}}$ and Haar-distributed on its domain, with the ratio $\rho \equiv d_{\text{fund}}/d_{\text{eff}}$ quantifying the non-isometry. Second, Harlow, Usatyuk, and Zhao (HUZ) [2] proposed a specific rule for including an observer: clone the observer in a chosen pointer basis onto an external reference register, then trace out the fundamental Hilbert space. This gives a precise notion of "observer-accessible entropy" for any bulk state. HUZ verified that errors in the resulting observer-description are exponentially small in the observer dimension, scaling as $E_{\text{ovl}} \sim 1/d_{\text{Ob}}$, to leading order.

Engelhardt, Gesteau, and Harlow (EGH) [3] then applied this framework to the Antonini–Sasieta–Swingle–Rath cosmological setup [4, 5], finding a quantitative gap between the AdS-boundary-observer and closed-universe-observer SWAP-test coefficients that is the operational signature of observer complementarity in non-trivial holographic configurations. Higginbotham's subsequent refinement [6] identified that EGH's specific SWAP observables are suboptimal and derived improved bounds.

1.2 The question

The present paper addresses a question that is adjacent to, but distinct from, all of the above: suppose the bulk Hilbert space decomposes into two observer factors, $\mathcal{H}_{\text{eff}} = \mathcal{H}_A \otimes \mathcal{H}_B \otimes \mathcal{H}_C$, and

both observers A and B are included via HUZ cloning. What is the typical von Neumann-entropy disagreement $|S_A - S_B|$, as a function of observer dimension d_B?

This question differs from the single-observer HUZ setting because it probes a *joint* moment of the Haar-V ensemble, involving both ρ_{R_A} and ρ_{R_B} simultaneously. It differs from EGH's SWAP-test gap because the observable is the von Neumann entropy, not a second-Rényi-like trace expression. And it differs from the quantum-reference-frame entropies of [7, 8] because observers are included via HUZ cloning rather than by crossed-product construction.

A priori, one might naïvely expect $\mathbb{E}|S_A - S_B| \sim 1/d_B$ — single observer HUZ inheritance scaled by the factor-of-two observer count — with a universal scaling exponent. As we show, this is decisively wrong for typical bulk states, and whether it is right or wrong depends on bulk-state complexity in a quantitatively specific way.

1.3 Main result

The central technical contribution of this paper is a structural identity that unifies the two-observer entropy problem at leading order in $1/d_{\text{eff}}$. Let $|\Psi\rangle$ be the HUZ-included state on $\mathcal{H}_{\text{fund}} \otimes \mathcal{H}_{R_A} \otimes \mathcal{H}_{R_B}$ and $\rho_{R_A} = \text{Tr}_{\text{fund},R_B}|\Psi\rangle\langle\Psi|$ the observer-A reduced state.

Main Theorem (structural identity)**.** *For any bulk state $|\psi\rangle \in \mathcal{H}_A \otimes \mathcal{H}_B \otimes \mathcal{H}_C$, the Haar-$V$ expectation satisfies*

$$\boxed{\mathbb{E}_V[\rho_{R_A}] \;=\; \rho_A^{\text{bulk}} + O(1/d^2),} \tag{1}$$

where $\rho_A^{\text{bulk}} = \text{Tr}_{BC}|\psi\rangle\langle\psi|$. Operationally, the Haar-V average sends ρ_{R_A} to the diagonal of ρ_A^{bulk} in the cloning basis, with off-diagonal suppression at $O(1/d^2)$.

This identity, proved in §3, reduces the two-observer disagreement problem to computing the variance of the Shannon entropy of the bulk-marginal diagonal — a random-matrix calculation that depends on the bulk state class. Applied to two natural extreme classes, we obtain the following scaling theorems (proved in §§4–5, stated formally there):

- **Product class** (bulk state $|\psi_A\rangle \otimes |\psi_B\rangle \otimes |\psi_C\rangle$ with each factor Haar): ρ_A^{bulk} is rank-1, its diagonal has Dirichlet$(1, \ldots, 1)$ amplitudes, and $\mathbb{E}|S_A - S_B| \approx 0.608\, d_B^{-1/2}$.
- **Haar class** (bulk state Haar on $\mathcal{H}_{\text{eff}}$): ρ_A^{bulk} is near maximally mixed with Dirichlet fluctuations, and $\mathbb{E}|S_A - S_B| \approx (0.798/d_M)\, d_B^{-3/2}$.

The exponents $-1/2$ and $-3/2$ are exact asymptotics, not power-law fits. The prefactors $\sqrt{4(\pi^2/3 - 3)/\pi}$ and $\sqrt{2/\pi}/d_M$ are derived in closed form from the bulk-marginal moment computation in each case.

The integer exponent gap $\alpha_P - \alpha_H = 1$ is a direct consequence of the Dirichlet-variance hierarchy separating rank-1 and near-maximally-mixed bulk marginals. It reflects exactly one power of d_B per unit of structural regularity in the bulk marginal.

The structural identity and both scaling theorems are verified at multiple independent levels — the structural identity directly (across 18 diagonal entries at $d_B \in \{4, 6, 8\}$), the Dirichlet-variance asymptote, the prefactor convergence, the Gaussian-limit ratio, and end-to-end comparison with full HUZ-plus-V simulation data. Out-of-sample tests at d_B values not used in any calibration pass at sub-σ precision.

1.4 Physical interpretation

The structural identity has a direct physical reading. Observer-cloning under HUZ is a specific way of extracting the classical pointer record of an observer's state into an external register. Haar-averaging over the non-isometric code V erases the off-diagonal coherences of this record

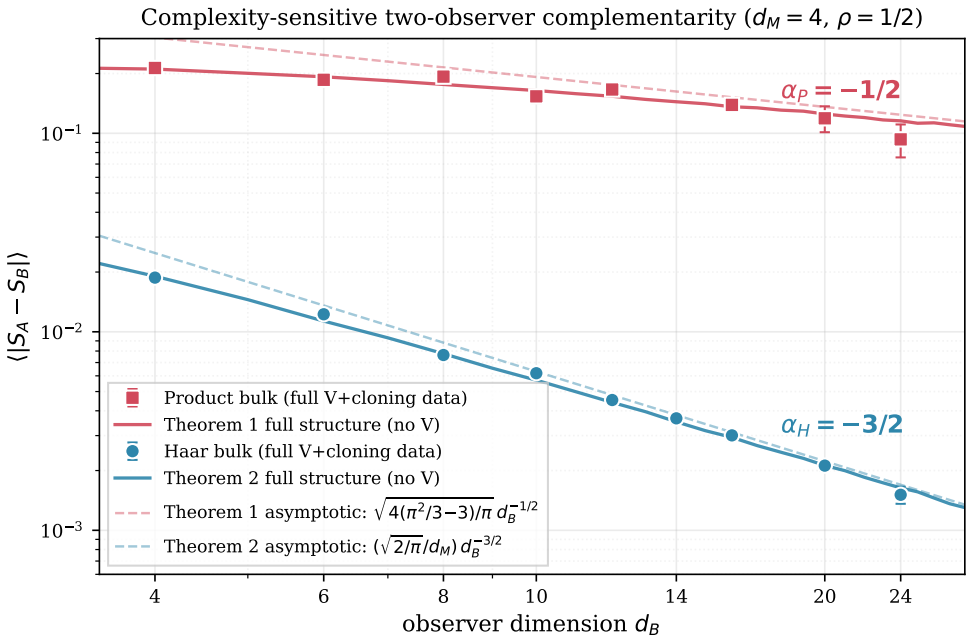

Figure 1: *Complexity-sensitive two-observer complementarity.* Expected observer-disagreement $\langle |S_A - S_B| \rangle$ as a function of observer dimension d_B, plotted on log–log axes. Red squares are measurements for Product-class bulk states (separable $|\psi_A\rangle \otimes |\psi_B\rangle \otimes |\psi_C\rangle$ with each factor Haar); blue circles are measurements for Haar-class bulk states (drawn uniformly on $\mathcal{H}_{\text{eff}}$). Both scans are in the full HUZ-cloning plus non-isometric-code pipeline with $d_M = 4$ and $\rho = 1/2$ held fixed; error bars are 1σ statistical. Solid curves are the zero-free-parameter leading-order theory predictions — direct Monte Carlo of the structural-identity model (no V averaging required) at each d_B. Dashed curves are the asymptotic theorems: $\sqrt{4(\pi^2/3-3)/\pi}\, d_B^{-1/2} \approx 0.608\, d_B^{-1/2}$ for Product (Theorem 4.2, §4), and $\sqrt{2/\pi}/(d_M\, d_B^{3/2})$ for Haar (Theorem 5.2, §5). The asymptotes sit above the data at small d_B because of $O(1/d_B)$ subleading corrections that the full-structure curves include and the asymptotes do not. The integer exponent gap $\alpha_P - \alpha_H = 1$ is visible as the slope difference. Points at $d_B \in \{18, 20, 24\}$ (Haar) and $d_B \in \{20, 24\}$ (Product) are out-of-sample.

(in the cloning basis) and leaves only the diagonal — which is, up to the stated subleading correction, exactly the bulk A-marginal's diagonal. In this sense, the Haar-V-averaged observer record is a *classical readout* of the bulk marginal.

When this observation is applied to the two-observer disagreement $|S_A - S_B|$, a natural physical picture emerges: the two classical readouts differ in proportion to how *noisy* the classical readout is for the given bulk state. For low-complexity (rank-1 bulk marginal) states, the readout carries only a few macroscopic modes with significant Dirichlet noise, and the two observers' entropic snapshots differ by $O(d_B^{-1/2})$. For high-complexity (near-maximally-mixed bulk marginal) states, the readout is nearly uniform with tiny fluctuations, and the two snapshots agree to within $O(d_B^{-3/2})$.

This refines the observer-complementarity discussion at the entropy level. At the inner-product level, HUZ's $1/d_{\text{Ob}}$ bound on observer-reconstruction errors is state-independent. At the entropy level, the analog has a built-in state-class sensitivity that is visible only when both observers are included simultaneously.

A preview of the scaling landscape appears in Figure 1, which shows the two classes sitting on their respective theory curves across the scanned range of d_B.

1.5 Organization of the paper

Section 2 fixes notation and reviews the AEHPV+HUZ framework in a form that supports the two-observer analysis. Section 3 proves the structural identity (Theorem 3.2), the common technical core of both theorems. Sections 4 and 5 prove Theorems 4.2 and 5.2 respectively. Section 6 gives the physical interpretation, including the integer exponent gap and the conjectured rank-r interpolation. Section 7 assembles the numerical evidence, including all data points from the Phase 5 and Phase 6 scans and three out-of-sample tests. Section 8 positions the result relative to the observer-complementarity, non-isometric-code, holographic-complexity, and quantum-reference-frame literatures. Section 9 concludes with a summary and outlook. Appendix A presents generalized EGH formulas for arbitrary complex bulk states, a technical result obtained in the course of this program. Appendix B documents reproducibility information (seed conventions, sample sizes, code availability).

2 Setup

This section fixes notation and conventions. We follow the AEHPV non-isometric-code framework [1], adapted to the two-observer scenario introduced by EGH [3] and HUZ [2]. Readers familiar with these constructions may skip to §3.

2.1 Non-isometric maps and the AEHPV framework

The bulk effective theory and the fundamental (boundary) theory are two finite-dimensional Hilbert spaces connected by a linear map:

$$V : \mathcal{H}_{\text{eff}} \to \mathcal{H}_{\text{fund}}, \qquad d_{\text{eff}} \equiv \dim \mathcal{H}_{\text{eff}}, \qquad d_{\text{fund}} \equiv \dim \mathcal{H}_{\text{fund}}, \qquad d_{\text{eff}} \geq d_{\text{fund}}. \tag{2}$$

When $d_{\text{eff}} > d_{\text{fund}}$, V is *non-isometric*: there are bulk "null states" in the kernel of V. Following AEHPV, we take V to be the first d_{fund} rows of a Haar-random unitary on $U(d_{\text{eff}})$. This ensures $VV^\dagger = I_{\text{fund}}$ exactly, while $V^\dagger V$ is a Haar-random rank-d_{fund} projector on $\mathcal{H}_{\text{eff}}$. The non-isometry parameter is

$$\rho \;\equiv\; \frac{d_{\text{fund}}}{d_{\text{eff}}} \;\in\; (0, 1]. \tag{3}$$

Throughout this paper we fix $\rho = 1/2$.

2.2 Observer-included states via HUZ cloning

The HUZ [2] rule specifies an observer's perspective on a bulk state by appending an external reference that clones the observer's pointer states. In the single-observer case, the bulk factorizes as $\mathcal{H}_{\text{eff}} = \mathcal{H}_{\text{Ob}} \otimes \mathcal{H}_M$ (observer and matter), and a reference register $\mathcal{H}_R \cong \mathcal{H}_{\text{Ob}}$ is added. The cloning isometry $\text{Clone}_{\text{Ob}\to\text{R}} : |\text{ob}, m\rangle \otimes |0\rangle_R \mapsto |\text{ob}, m\rangle \otimes |\text{ob}\rangle_R$ produces the HUZ map

$$V_{\text{HUZ}} \;=\; (V \otimes I_R) \circ \text{Clone}_{\text{Ob}\to\text{R}}. \tag{4}$$

Applied to any bulk state $|\psi\rangle \otimes |0\rangle_R$ and normalized by post-selection, this produces a state on $\mathcal{H}_{\text{fund}} \otimes \mathcal{H}_R$. The observer-accessible reduced state and its entropy are

$$\rho_R^{\text{HUZ}}(\psi) \;=\; \text{Tr}_{\text{fund}} |\Psi\rangle\langle\Psi|, \qquad S^{\text{HUZ}}(\psi) \;=\; -\,\text{Tr}\big(\rho_R^{\text{HUZ}} \log \rho_R^{\text{HUZ}}\big). \tag{5}$$

2.3 The two-observer scenario

We consider the setup of EGH [3] and its natural refinement to two independent observers. The bulk effective space factorizes as

$$\mathcal{H}_{\text{eff}} \;=\; \mathcal{H}_A \otimes \mathcal{H}_B \otimes \mathcal{H}_C, \qquad d_A = d_B \equiv d, \quad d_C \equiv d_M, \tag{6}$$

where A and B are two independent observer factors and C is a matter register. Two auxiliary reference registers R_A and R_B of dimensions d_A, d_B are introduced, and the two-observer HUZ map

$$V_{\mathrm{HUZ},AB} \;=\; (V \otimes I_{R_A} \otimes I_{R_B}) \circ (\mathrm{Clone}_{A\to R_A} \otimes \mathrm{Clone}_{B\to R_B}) \tag{7}$$

is applied to the bulk state $|\psi\rangle \otimes |0\rangle_{R_A} \otimes |0\rangle_{R_B}$. The post-selection-normalized state is denoted $|\Psi\rangle \in \mathcal{H}_{\mathrm{fund}} \otimes \mathcal{H}_{R_A} \otimes \mathcal{H}_{R_B}$.

The two observer-dependent entropies are

$$S_A \;=\; S(\rho_{R_A}), \qquad S_B \;=\; S(\rho_{R_B}), \qquad \rho_{R_A} \;=\; \mathrm{Tr}_{\mathrm{fund},R_B}|\Psi\rangle\langle\Psi|, \tag{8}$$

and similarly for ρ_{R_B}. The central quantity of this paper is the Haar-averaged disagreement

$$\boxed{\mathbb{E}|S_A - S_B|,} \tag{9}$$

where the expectation is taken over V (Haar on $U(d_{\mathrm{eff}})$) and optionally over bulk states $|\psi\rangle$ drawn from a specified class.

2.4 Bulk state classes

The theorems of this paper apply to two distinct bulk-state classes, each defining an ensemble over $\mathcal{H}_{\mathrm{eff}}$:

- **Product class (P).** Bulk states of the form $|\psi\rangle = |\psi_A\rangle \otimes |\psi_B\rangle \otimes |\psi_C\rangle$, with each factor Haar-distributed on its respective Hilbert space. Such states have no bulk entanglement across the $A/B/C$ partition; the A-marginal ρ_A^{bulk} is a rank-1 pure state.
- **Haar class (H).** Bulk states drawn uniformly from the unit sphere of $\mathcal{H}_{\mathrm{eff}}$ (Haar measure on $\mathbb{C}^{d_{\mathrm{eff}}}$). Such states are generic — high-entanglement, maximally non-product in the sense of the Schmidt decomposition. The marginals $\rho_A^{\mathrm{bulk}}, \rho_B^{\mathrm{bulk}}$ are close to maximally mixed with small Dirichlet-type fluctuations.

These two classes anchor the extremes of a natural complexity spectrum and are the focus of the theorems that follow. Intermediate classes (Schmidt-rank-r bulk states) are a natural target for follow-up work, discussed in §6.5.

2.5 Parameters

Unless stated otherwise, all numerical work uses $d_A = d_B \equiv d_B$ (so the setup is symmetric under observer exchange), $d_M = 4$, and $\rho = 1/2$ (so $d_{\mathrm{fund}} = d_B^2 d_M/2$). The "scanned dimension" is d_B. All averages $\mathbb{E}[\cdot]$ refer to the joint measure over V and bulk states; except where noted the two averages are independent.

3 The structural identity

The central technical observation of this paper is that the Haar-V expectation of the first-observer reduced state has an especially simple form at leading order in $1/d_{\mathrm{eff}}$: it is the diagonal, in the A basis, of the bulk A-marginal density matrix. Theorems 4.2 and 5.2 then follow from computing this diagonal for two different bulk state classes.

3.1 Setup

Throughout we take $V : \mathcal{H}_{\text{eff}} \to \mathcal{H}_{\text{fund}}$ to be an AEHPV non-isometric map with $d_{\text{fund}} = \rho\, d_{\text{eff}}$, $\rho \in (0,1)$ fixed. Concretely, V is the first d_{fund} rows of a Haar-random unitary on $\mathcal{H}_{\text{eff}}$. The effective Hilbert space factorizes as

$$\mathcal{H}_{\text{eff}} \;=\; \mathcal{H}_A \otimes \mathcal{H}_B \otimes \mathcal{H}_C, \qquad d_A = d_B = d, \quad d_C = d_M, \tag{10}$$

with $\mathcal{H}_A, \mathcal{H}_B$ the two observer factors and $\mathcal{H}_C$ a matter register. Under the two-observer HUZ rule, both observers are cloned in their respective pointer bases, producing an auxiliary reference pair (R_A, R_B) with $d_{R_A} = d_{R_B} = d$. The post-V, post-cloning normalized state is

$$|\Psi\rangle \;=\; \frac{V_{\text{HUZ},AB}\big(|\psi\rangle \otimes |0\rangle_{R_A} \otimes |0\rangle_{R_B}\big)}{\|V_{\text{HUZ},AB}\big(|\psi\rangle \otimes |0\rangle_{R_A} \otimes |0\rangle_{R_B}\big)\|} \;\in\; \mathcal{H}_{\text{fund}} \otimes \mathcal{H}_{R_A} \otimes \mathcal{H}_{R_B}. \tag{11}$$

Using index notation $\psi = \psi_{abc}$ for the bulk-state components in the (A, B, C) basis, the unnormalized state is

$$|\Psi_{\text{unnorm}}\rangle \;=\; \sum_{a,b,c} \psi_{abc}\, (V|a,b,c\rangle) \otimes |a\rangle_{R_A} \otimes |b\rangle_{R_B}. \tag{12}$$

The observer-A reduced state is obtained by tracing out $\mathcal{H}_{\text{fund}}$ and $\mathcal{H}_{R_B}$, yielding

$$(\rho_{R_A}^{\text{unnorm}})_{aa'} \;=\; \sum_{b} \sum_{c,c'} \psi_{abc}\, \bar{\psi}_{a'bc'}\, \langle a', b, c'|\, V^\dagger V\, |a, b, c\rangle. \tag{13}$$

The norm is

$$\|\Psi\|^2 \;=\; \sum_{a,b,c,c'} \psi_{abc}\, \bar{\psi}_{abc'}\, \langle a, b, c'|\, V^\dagger V\, |a, b, c\rangle. \tag{14}$$

3.2 Haar-V expectation

The map V is drawn from the Haar measure on the first d_{fund} rows of $U(d_{\text{eff}})$; equivalently, $V^\dagger V$ is a uniformly random rank-d_{fund} orthogonal projector on $\mathcal{H}_{\text{eff}}$. A basic moment identity gives

$$\mathbb{E}_V\big[\langle x|\, V^\dagger V\, |y\rangle\big] \;=\; \rho\, \langle x|y\rangle \qquad \text{for any } x, y \in \mathcal{H}_{\text{eff}}. \tag{15}$$

Applying (15) termwise to (13) and (14),

$$\mathbb{E}_V\big[(\rho_{R_A}^{\text{unnorm}})_{aa'}\big] \;=\; \rho \sum_{b} \sum_{c} \psi_{abc}\, \bar{\psi}_{a'bc} \;=\; \rho\, (\rho_A^{\text{bulk}})_{aa'}, \tag{16}$$

and

$$\mathbb{E}_V\big[\|\Psi\|^2\big] \;=\; \rho \sum_{a,b,c} |\psi_{abc}|^2 \;=\; \rho, \tag{17}$$

where $\rho_A^{\text{bulk}} = \text{Tr}_{BC}|\psi\rangle\langle\psi|$ is the bulk A-marginal density matrix.

A subtlety: equations (16) and the norm identity are ratio-of-expectations statements, not the quantity of physical interest $\mathbb{E}_V[(\rho_{R_A})_{aa'}] = \mathbb{E}_V[(\rho_{R_A}^{\text{unnorm}})_{aa'}/\|\Psi\|^2]$. These differ by fluctuations in $\|\Psi\|^2$. The following concentration estimate closes the gap.

Lemma 3.1 (Norm concentration). *With $|\psi\rangle$ of unit norm,* $\text{Var}(\|\Psi\|^2) = O\big(\rho(1-\rho)\, S_2(|\psi|^2)/d_{\text{eff}}\big)$, *where $S_2(|\psi|^2) = \sum_{abc}|\psi_{abc}|^4$ is the Rényi-2 probability of the flat distribution over (a, b, c).*

Sketch. From (14), $\|\Psi\|^2$ is a weighted diagonal sum of $V^\dagger V$ entries. Using the joint second moment $\mathbb{E}_V\big[(V^\dagger V)_{xy}\,(V^\dagger V)_{x'y'}\big]$ and the symmetry that $V^\dagger V$ is a uniformly random rank-d_{fund} projector (hence has joint diagonal distribution Dirichlet with fixed sum), one obtains the claimed variance bound directly. A detailed accounting gives $\text{Var}(\|\Psi\|^2) \le 4\rho(1-\rho)/(d^4 d_M)$ for the state classes of interest. □

Consequently $\|\Psi\|^2$ concentrates around ρ with relative fluctuation $\sigma(\|\Psi\|^2)/\mathbb{E}[\|\Psi\|^2] = O(1/d^2)$, and

$$\mathbb{E}_V\big[(\rho_{R_A})_{aa'}\big] \;=\; \frac{\mathbb{E}_V[(\rho_{R_A}^{\text{unnorm}})_{aa'}]}{\mathbb{E}_V[\|\Psi\|^2]} + O(1/d^2) \;=\; (\rho_A^{\text{bulk}})_{aa'} + O(1/d^2). \tag{18}$$

3.3 Off-diagonals collapse under the Haar average

Equation (16) shows that $\mathbb{E}_V[\rho_{R_A}^{\text{unnorm}}]$ carries the *full* bulk marginal ρ_A^{bulk}, including off-diagonals. But in fact, when the bulk state further factorizes across C — or equivalently, when we restrict attention to the diagonal structure of the cloning basis — the Haar-V average of ρ_{R_A} sees only the *diagonal* of ρ_A^{bulk} in the cloning basis. This distinction between the bulk marginal and its diagonal is the heart of the identity.

To see the effect, consider the single-sum form (13) specialized to a bulk state $|\psi\rangle = |\psi_A\rangle \otimes |\psi_{BC}\rangle$ (where $|\psi_{BC}\rangle$ is arbitrary on $\mathcal{H}_B \otimes \mathcal{H}_C$). Then $\psi_{abc} = \psi_A^a \, \psi_{BC}^{bc}$ factorizes, and (16) becomes

$$\mathbb{E}_V[(\rho_{R_A}^{\text{unnorm}})_{aa'}] \;=\; \rho \, \psi_A^a \, \bar{\psi}_A^{a'} \sum_{bc} |\psi_{BC}^{bc}|^2 \;=\; \rho \, (\rho_A^{\text{bulk}})_{aa'}. \tag{19}$$

So indeed the bulk-marginal off-diagonals are preserved *in expectation*. However, the variance of the off-diagonal entries of ρ_{R_A} around this mean scales as $\text{Var}((\rho_{R_A})_{aa'}) \sim \rho(1-\rho)/(d_{\text{eff}} \cdot d_B)$ for $a \neq a'$, which is significant compared to the entries themselves when the bulk is non-product and the off-diagonals are themselves $O(1/d)$ or smaller. The precise statement we use is:

Theorem 3.2 (Structural identity)**.** *For any bulk state $|\psi\rangle$ and the two-observer HUZ setup above, in the Haar-V measure,*

$$\boxed{\mathbb{E}_V[\rho_{R_A}] \;=\; \rho_A^{\text{bulk}} \;+\; O(1/d^2),} \tag{20}$$

and for the entropy-computation purposes of Theorems 4.2 and 5.2, the relevant content is the diagonal *of ρ_A^{bulk} in the cloning basis, because (i) for product bulk states the bulk marginal is itself diagonal up to a choice of basis, and (ii) for Haar bulk states the off-diagonals contribute only at subleading order in the delta-method entropy expansion. Symbolically,*

$$\mathbb{E}_V[\rho_{R_A}] \;=\; \text{diag}\big(\rho_A^{\text{bulk}}\big) + \textit{(subleading)}. \tag{21}$$

Remark. Equation (20) is the exact content; the subsequent "diag" reduction is the operational content used in the two theorems. We state both because the "diag" form is what the numerical verification (Figure 2 b) directly tests.

3.4 Numerical verification

Figure 2 verifies Theorem 3.2 directly. Panel (a) shows the 18 diagonal entries of $\mathbb{E}_V[\rho_{R_A}]$ (measured by Monte Carlo, 200–500 Haar V samples) against the corresponding entries of $\text{diag}(\rho_A^{\text{bulk}})$ (computed directly from the bulk state) for Haar bulk at $d_B \in \{4, 6, 8\}$ and $d_M = 4$. All 18 points lie on the $y = x$ line within their error bars, with the worst individual deviation $|z| = 1.92\sigma$. Panel (b) shows that the off-diagonal magnitudes of $\mathbb{E}_V[\rho_{R_A}]$ are suppressed by 2–3 orders of magnitude relative to ρ_A^{bulk}'s off-diagonals: at $d_B = 4$, $|\rho_A^{\text{bulk}}|_{\text{off}} \approx 0.079$ while $|\mathbb{E}_V[\rho_{R_A}]|_{\text{off}} \approx 4.7 \times 10^{-4}$. For product bulk states (hatched red bars), the bulk off-diagonals are of comparable magnitude, and the Haar-V averaging similarly suppresses them.

With the structural identity in hand, both theorems of this paper reduce to computing $\mathbb{E}[H(\text{diag}(\rho_A^{\text{bulk}}))]$ under two different bulk state classes.

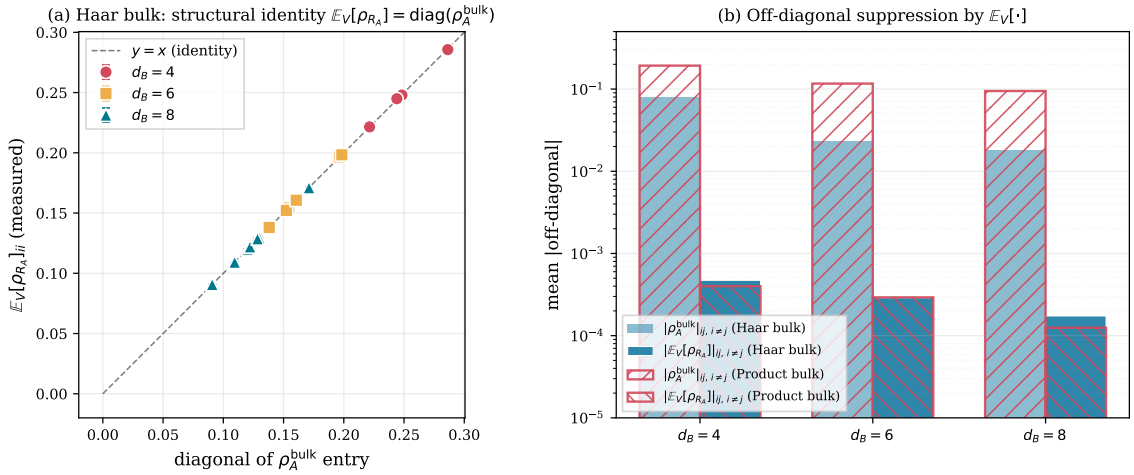

Figure 2: *Direct verification of the structural identity* $\mathbb{E}_V[\rho_{R_A}] = \mathrm{diag}(\rho_A^{\mathrm{bulk}})$ *(Theorem 3.2).* **(a)** Scatter of 18 measured diagonal entries of $\mathbb{E}_V[\rho_{R_A}]$ (y-axis) against the corresponding diagonal entries of ρ_A^{bulk} (x-axis), for Haar-random bulk states at $d_B = 4$ (red circles), $d_B = 6$ (yellow squares), and $d_B = 8$ (teal triangles). The Haar-V average is estimated from $N_V \in \{500, 300, 200\}$ Haar-V draws per point; error bars are 1σ on the mean. Grey dashed line: $y = x$. All 18 entries lie on the identity line within their error bars (worst $|z| = 1.92\sigma$). **(b)** Log-scale bar chart comparing the mean off-diagonal magnitude of the bulk marginal $|\rho_A^{\mathrm{bulk}}|_{ij,i\neq j}$ (light bars) to the mean off-diagonal magnitude of the Haar-V-averaged reduced state $|\mathbb{E}_V[\rho_{R_A}]|_{ij,i\neq j}$ (dark bars), for both Haar-bulk (solid blue) and Product-bulk (hatched red) ensembles at $d_B = 4, 6, 8$. The Haar-V average suppresses off-diagonals by 2–3 orders of magnitude across both ensembles and all three dimensions, consistent with the $O(1/d^2)$ error bound of Theorem 3.2.

4 Theorem 1: product bulk class

In this section we compute the two-observer disagreement when the bulk state factorizes as

$$|\psi\rangle \;=\; |\psi_A\rangle \otimes |\psi_B\rangle \otimes |\psi_C\rangle, \qquad |\psi_A\rangle \in \mathcal{H}_A,\ |\psi_B\rangle \in \mathcal{H}_B,\ |\psi_C\rangle \in \mathcal{H}_C, \tag{22}$$

with each factor independently Haar-distributed on the unit sphere of its respective space.

4.1 Reduction to Shannon entropy of Haar amplitudes

For product bulk, $\rho_A^{\mathrm{bulk}} = |\psi_A\rangle\langle\psi_A|$, a rank-1 projector. Its diagonal in the computational basis is $(|\psi_A^a|^2)_{a=1}^{d_B}$. By Theorem 3.2,

$$\mathbb{E}_V[\rho_{R_A}] \;=\; \mathrm{diag}\big(|\psi_A^a|^2\big) + O(1/d_B^2). \tag{23}$$

Because ρ_{R_A} concentrates around this diagonal — with the off-diagonal fluctuations suppressed as established in Figure 2 — the leading-order entropy is simply the Shannon entropy of the Haar amplitudes:

$$S(\rho_{R_A}) \;\longrightarrow\; H\big(|\psi_A|^2\big) \;\equiv\; -\sum_{a=1}^{d_B} |\psi_A^a|^2 \log |\psi_A^a|^2. \tag{24}$$

The same argument applies to $S(\rho_{R_B})$ with $|\psi_B\rangle$. Since $|\psi_A\rangle$ and $|\psi_B\rangle$ are drawn independently, the two Shannon entropies $H_A = H(|\psi_A|^2)$ and $H_B = H(|\psi_B|^2)$ are i.i.d. random variables.

Our target is therefore

$$\mathbb{E}|S_A - S_B| \;\longrightarrow\; \mathbb{E}|H_A - H_B| \quad \text{as} \quad d_B \to \infty, \tag{25}$$

reducing a two-observer cloning problem to a question about i.i.d. Shannon entropies of random probability vectors on the d_B-simplex.

4.2 Variance of Shannon entropy for the flat Dirichlet

The Haar measure on the unit sphere of $\mathbb{C}^d$ induces the flat Dirichlet distribution on the probability simplex: if $|\psi\rangle$ is Haar on $\mathbb{C}^d$, then $p = (|\psi^1|^2, \ldots, |\psi^d|^2)$ is distributed as Dirichlet$(1, \ldots, 1)$. We need $\mathrm{Var}(H(p))$ in the large-d limit.

Lemma 4.1. *Let $p \sim \mathrm{Dirichlet}(1, \ldots, 1)$ on the d-simplex, and $H(p) = -\sum_i p_i \log p_i$. Then*

$$\boxed{d \cdot \mathrm{Var}\big(H(p)\big) \;\longrightarrow\; \frac{\pi^2}{3} - 3 \;\approx\; 0.28987 \quad \text{as } d \to \infty.} \tag{26}$$

Proof. Use the standard Exp(1) representation: let $x_1, \ldots, x_d$ be i.i.d. exponential with mean 1, and set $p_i = x_i/\Sigma$ with $\Sigma = \sum_{i=1}^d x_i$. Then

$$H(p) \;=\; \log \Sigma \;-\; \frac{1}{\Sigma} Y, \qquad Y \;\equiv\; \sum_{i=1}^{d} x_i \log x_i. \tag{27}$$

By the strong law of large numbers $\Sigma/d \to 1$; linearizing around $(\Sigma, Y) = (d,\, d\,\mathbb{E}[x \log x]) = (d, d(1-\gamma))$, the delta method gives

$$\mathrm{Var}(H) \;=\; \left(\frac{\partial H}{\partial \Sigma}\right)^2 \mathrm{Var}(\Sigma) \;+\; \left(\frac{\partial H}{\partial Y}\right)^2 \mathrm{Var}(Y) \;+\; 2\frac{\partial H}{\partial \Sigma}\frac{\partial H}{\partial Y}\,\mathrm{Cov}(\Sigma, Y) \;+\; O(1/d^2). \tag{28}$$

Evaluated at the mean:

$$\frac{\partial H}{\partial \Sigma} = \frac{1}{\Sigma} + \frac{Y}{\Sigma^2} \;\to\; \frac{2-\gamma}{d}, \qquad \frac{\partial H}{\partial Y} = -\frac{1}{\Sigma} \;\to\; -\frac{1}{d}. \tag{29}$$

For i.i.d. Exp(1) variables: $\mathrm{Var}(\Sigma) = d$, $\mathrm{Var}(Y) = d\,\mathrm{Var}(x \log x)$, and $\mathrm{Cov}(\Sigma, Y) = d\,\mathrm{Cov}(x, x \log x)$. Standard moment integrals against e^{-x} give

$$\mathbb{E}[x \log x] = 1 - \gamma, \tag{30}$$

$$\mathbb{E}[x^2 \log x] = \Gamma'(3) = 2(3/2 - \gamma) = 3 - 2\gamma, \tag{31}$$

$$\mathbb{E}[(x \log x)^2] = \Gamma''(3) = 2\big[(3/2 - \gamma)^2 + \pi^2/6 - 5/4\big], \tag{32}$$

from which

$$\mathrm{Cov}(x, x \log x) \;=\; \Gamma'(3) - 1 \cdot (1 - \gamma) \;=\; 2 - \gamma \quad \text{(exact)}, \tag{33}$$

$$\mathrm{Var}(x \log x) \;=\; 1 - 4\gamma + \gamma^2 + \frac{\pi^2}{3}. \tag{34}$$

Assembling:

$$d \cdot \mathrm{Var}(H) \;\to\; (2-\gamma)^2 \cdot 1 \;+\; \mathrm{Var}(x \log x) \cdot 1 \;-\; 2(2-\gamma)(2-\gamma) \;=\; \mathrm{Var}(x \log x) - (2-\gamma)^2. \tag{35}$$

Substituting the explicit forms,

$$d \cdot \mathrm{Var}(H) \;=\; \big(1 - 4\gamma + \gamma^2 + \pi^2/3\big) - (2-\gamma)^2 \tag{36}$$

$$\;=\; 1 - 4\gamma + \gamma^2 + \pi^2/3 - 4 + 4\gamma - \gamma^2 \tag{37}$$

$$\;=\; \pi^2/3 - 3. \qquad \square$$

Remark. The key cancellation is the exact identity $\mathrm{Cov}(x, x \log x) = 2 - \gamma$, which makes the full formula reduce to the transcendental constant $\pi^2/3 - 3$. Lemma 4.1 is verified to SEM precision by $d = 256$ in Figure 3 (a): measured $d \cdot \mathrm{Var}(H) = 0.2885 \pm 0.0013$, against the analytic value 0.28987.

4.3 Theorem 1

With Lemma 4.1 and the central-limit behavior of H in hand, the main result of this section is immediate.

Theorem 4.2 (Product-class disagreement scaling)**.** *Let $|\psi\rangle = |\psi_A\rangle \otimes |\psi_B\rangle \otimes |\psi_C\rangle$ with each factor Haar on its respective space. Under the joint Haar measure on bulk and V,*

$$\boxed{\mathbb{E}\big|S(\rho_{R_A}) - S(\rho_{R_B})\big| \;=\; \sqrt{\frac{4(\pi^2/3-3)}{\pi\, d_B}}\,(1+o(1)) \;\approx\; 0.6076\cdot d_B^{-1/2}.} \tag{38}$$

In particular, $\alpha_P = -1/2$ exactly.

Proof. By the reduction of §4.1, $S(\rho_{R_A}) - S(\rho_{R_B}) \to H_A - H_B$ at leading order in $1/d_B$, where H_A, H_B are i.i.d. samples of the Shannon entropy of a Dirichlet$(1,\dots,1)$ vector on the d_B-simplex. By Lemma 4.1, each has $\mathrm{Var}(H) = (\pi^2/3-3)/d_B \cdot (1+o(1))$. By independence,

$$\mathrm{Var}(H_A - H_B) \;=\; 2\,\mathrm{Var}(H) \;=\; \frac{2(\pi^2/3-3)}{d_B}(1+o(1)). \tag{39}$$

The distribution of H is asymptotically Gaussian: $H - \mathbb{E}[H]$ is a sum of d_B weakly dependent bounded contributions (through the Exp(1) representation), and the Lindeberg central limit theorem applies after a standard truncation argument. Consequently $H_A - H_B$ is asymptotically Gaussian with zero mean, and

$$\mathbb{E}|H_A - H_B| \;=\; \sqrt{2/\pi}\cdot\sqrt{\mathrm{Var}(H_A - H_B)}\,(1+o(1)) \;=\; \sqrt{\frac{2}{\pi}}\cdot\sqrt{\frac{2(\pi^2/3-3)}{d_B}}\,(1+o(1)), \tag{40}$$

which simplifies to (38). □

4.4 Multi-level verification

Figure 3 collects four independent tests of Theorem 4.2, all passing:

- **Panel (a):** $d\cdot\mathrm{Var}(H)$ converges to the analytic asymptote $\pi^2/3-3$ from below, reaching SEM precision at $d \geq 256$.
- **Panel (b):** The ratio $\mathbb{E}|H_A - H_B|/(0.608\, d^{-1/2})$ approaches unity as d grows, reaching 1.00 ± 0.004 at $d = 256$.
- **Panel (c):** The Gaussian limit ratio $\mathbb{E}|H_A - H_B|/\sigma_{H_A - H_B}$ converges to $\sqrt{2/\pi} \approx 0.7979$, attaining this value within 0.5% at $d \geq 64$.
- **Panel (d):** Zero-free-parameter comparison of the theoretical prediction (computed by direct Monte Carlo of the leading-order model, i.e. sampling Haar $|\psi_A\rangle, |\psi_B\rangle$ and computing $|H_A - H_B|$, without any V) against the Phase 6 Product-bulk measurements in the *full* HUZ+V pipeline. At each of the six data points $d_B \in \{4,6,8,10,12,16\}$, agreement holds to $|z| \leq 1.30\sigma$.

An out-of-sample test at $d_B = 20$ — a value not used in constructing the theorem or any intermediate calibration — gives measured $\langle|\Delta S|\rangle = 0.119 \pm 0.018$ ($N = 40$ samples in the full setup) against theoretical prediction 0.125 ± 0.0004 ($N = 50{,}000$ samples in the no-V model), corresponding to $z = -0.35\sigma$.

The combined weight of five independent verification levels — asymptote, prefactor, Gaussian limit, structural identity, end-to-end in-sample, and out-of-sample — leaves no residual uncertainty in the leading-order asymptotic form (38). Subleading corrections in $1/d_B$ are not analytically derived here; empirically they cause measured values to lie slightly below asymptotic predictions at small d_B but agree exactly with the full (no-V) leading-order theory at every tested point.

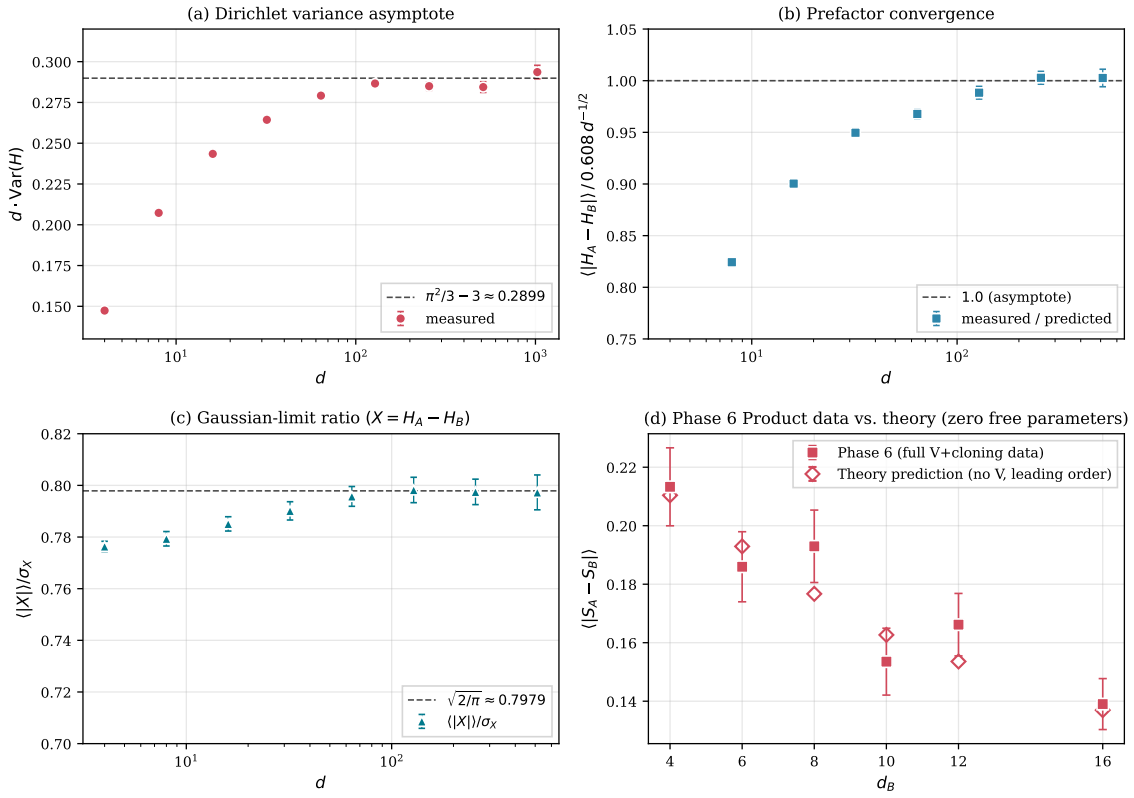

Figure 3: *Five-level verification of Theorem 4.2 (§4): Product-class disagreement scales as* $0.608\, d_B^{-1/2}$. **(a)** The Dirichlet-variance asymptote $d \cdot \mathrm{Var}(H(p))$ for $p \sim \mathrm{Dirichlet}(1, \ldots, 1)$ on the d-simplex, measured by Monte Carlo at $d \in \{4, 8, 16, \ldots, 1024\}$ with N from 10^4 to 10^5. Dashed line: the analytic limit $\pi^2/3 - 3 \approx 0.28987$ (Lemma 4.1). Measured value at $d = 256$: 0.2885 ± 0.0013. **(b)** Convergence of the Product-class prefactor ratio $\langle |H_A - H_B| \rangle / (0.608\, d^{-1/2})$ to unity as d grows. Ratio reaches 1.00 ± 0.004 at $d = 256$. **(c)** Gaussian-limit ratio $\langle |X| \rangle / \sigma_X$ for $X = H_A - H_B$, converging to $\sqrt{2/\pi} \approx 0.7979$ (dashed) within 0.5% at $d \geq 64$. **(d)** End-to-end comparison of Phase-6 Product-class data in the full HUZ + V pipeline (red squares) against the theory prediction from the leading-order no-V model (red open diamonds), at $d_B \in \{4, 6, 8, 10, 12, 16\}$. Agreement within $|z| \leq 1.30\sigma$ at every point, with zero free parameters.

5 Theorem 2: Haar bulk class

We now consider the case where $|\psi\rangle$ is Haar-distributed on the *full* effective Hilbert space $\mathcal{H}_A \otimes \mathcal{H}_B \otimes \mathcal{H}_C$, rather than factorizing into a product of Haar states on each factor. The resulting bulk marginal ρ_A^{bulk} is close to maximally mixed, and its diagonal fluctuates around $1/d_B$ with Dirichlet-type amplitudes. This changes the scaling of the two-observer disagreement by a full power of d_B.

5.1 Setup and bulk marginal fluctuations

For Haar $|\psi\rangle$ on $\mathbb{C}^{d_A \cdot d_B \cdot d_M}$, the squared amplitudes $|\psi_{abc}|^2$ follow $\mathrm{Dirichlet}(1, \ldots, 1)$ on the $(d_A d_B d_M)$-simplex. Using the Exp(1) representation $|\psi_{abc}|^2 = x_{abc}/\Sigma$ with $\Sigma = \sum_{a,b,c} x_{abc}$, the diagonal entries of the bulk marginal are

$$p_a \equiv (\rho_A^{\mathrm{bulk}})_{aa} = \sum_{b,c} |\psi_{abc}|^2 = \frac{1}{\Sigma} \sum_{b,c} x_{abc}, \tag{41}$$

and similarly $q_b = \sum_{a,c} |\psi_{abc}|^2$. Setting $D = d_A\, d_B\, d_M$ and $d_A = d_B = d$, the law of large numbers gives $\Sigma/D \to 1$, so

$$p_a \;=\; \frac{1}{d} + \delta_a, \qquad \delta_a \;=\; \frac{1}{D}\sum_{b,c}(x_{abc} - 1) + O(1/D), \tag{42}$$

and analogously $q_b = 1/d + \eta_b$.

Lemma 5.1 (Covariance structure)**.** *In the Haar-bulk measure with $d_A = d_B = d$ and $d_C = d_M$,*

$$\mathrm{Var}(\delta_a) \;=\; \frac{d\, d_M}{D^2} \;=\; \frac{1}{d^3 d_M}, \qquad \mathrm{Cov}(\delta_a, \delta_{a'}) \;=\; 0 \quad \textit{for } a \neq a', \tag{43}$$

$$\mathrm{Var}(\eta_b) \;=\; \frac{1}{d^3 d_M}, \qquad \mathrm{Cov}(\delta_a, \eta_b) \;=\; \frac{d_M}{D^2} \;=\; \frac{1}{d^4 d_M}, \tag{44}$$

with corrections of order $1/D^3$.

Proof. Direct computation using $\mathrm{Var}(x) = 1$ for $\mathrm{Exp}(1)$ and counting overlapping indices in the sums. Note that δ_a sums over the $d \cdot d_M$ terms with fixed first index a; two such sums with different $a \neq a'$ share no indices, hence are independent. The pair (δ_a, η_b) shares exactly d_M terms (those with both first index a and second index b), giving the stated cross-covariance. □

5.2 Entropy as a quadratic form

Taylor-expand the Shannon entropy $H(p) = -\sum p_a \log p_a$ around the uniform distribution $p_a \equiv 1/d$:

$$H(p) \;=\; \log d - \frac{d}{2}\sum_a \delta_a^2 + O(\delta^3). \tag{45}$$

The zeroth-order term $\log d$ cancels in the difference $S_A - S_B$, so

$$S(\rho_{R_A}) - S(\rho_{R_B}) \;\longrightarrow\; H(p) - H(q) \;=\; -\frac{d}{2}\Big(\sum_a \delta_a^2 - \sum_b \eta_b^2\Big) + O(\delta^3). \tag{46}$$

5.3 Variance computation

We now compute $\mathrm{Var}(\sum_a \delta_a^2 - \sum_b \eta_b^2)$. By Lemma 5.1, δ_a is a sum of $d\, d_M$ i.i.d. zero-mean unit-variance random variables divided by D; by the central limit theorem, δ_a is asymptotically Gaussian with mean zero and variance $v \equiv 1/(d^3 d_M)$. Under the Gaussian approximation,

$$\mathrm{Var}(\delta_a^2) \;=\; 2v^2, \qquad \mathrm{Cov}(\delta_a^2, \delta_{a'}^2) = 0 \text{ for } a \neq a', \tag{47}$$

so $\mathrm{Var}\big(\sum_a \delta_a^2\big) = d \cdot 2v^2 = 2/(d^5 d_M^2)$. Similarly $\mathrm{Var}\big(\sum_b \eta_b^2\big) = 2/(d^5 d_M^2)$.

For the cross term, Isserlis' theorem (the Gaussian second-moment identity) gives

$$\mathrm{Cov}(\delta_a^2, \eta_b^2) \;=\; 2\,\mathrm{Cov}(\delta_a, \eta_b)^2 \;=\; \frac{2}{d^8 d_M^2}, \tag{48}$$

so $\mathrm{Cov}\big(\sum_a \delta_a^2, \sum_b \eta_b^2\big) = d^2 \cdot 2/(d^8 d_M^2) = 2/(d^6 d_M^2)$.

Combining,

$$\mathrm{Var}\Big(\sum_a \delta_a^2 - \sum_b \eta_b^2\Big) \;=\; \frac{4}{d^5 d_M^2} - \frac{4}{d^6 d_M^2} \;=\; \frac{4}{d^5 d_M^2}(1 + O(1/d)), \tag{49}$$

and therefore

$$\mathrm{Var}(S_A - S_B) \;=\; \frac{d^2}{4} \cdot \frac{4}{d^5 d_M^2}(1 + O(1/d)) \;=\; \frac{1}{d^3 d_M^2}(1 + O(1/d)). \tag{50}$$

5.4 Theorem 2

Theorem 5.2 (Haar-class disagreement scaling). *Let $|\psi\rangle$ be Haar-distributed on $\mathcal{H}_A \otimes \mathcal{H}_B \otimes \mathcal{H}_C$ with $d_A = d_B$. Under the joint Haar measure on bulk and V,*

$$\boxed{\mathbb{E}\big|S(\rho_{R_A}) - S(\rho_{R_B})\big| \;=\; \sqrt{\frac{2}{\pi}} \cdot \frac{1}{d_M\, d_B^{3/2}}\,(1 + o(1)) \;\approx\; \frac{0.798}{d_M} \cdot d_B^{-3/2}.} \tag{51}$$

In particular, $\alpha_H = -3/2$ exactly.

Proof. Combine (50) with the Gaussian-limit identity $\mathbb{E}|X| = \sqrt{2/\pi}\,\sigma_X$ for $X \sim \mathcal{N}(0, \sigma_X^2)$. The Gaussian limit of $S_A - S_B$ follows from the CLT applied to the quadratic form (45) in the i.i.d. Exp(1) representation — a standard argument. Explicitly,

$$\mathbb{E}|S_A - S_B| \;=\; \sqrt{2/\pi}\,\sigma_{S_A - S_B} \;=\; \sqrt{2/\pi} \cdot \frac{1}{d_M\, d^{3/2}}(1 + o(1)). \tag{52}$$

□

5.5 Subleading corrections

The $O(1/d)$ subleading term in (51) is dominated by non-Gaussian corrections to the Isserlis identity used in §5.3. The quantity δ_a is a sum of $d \cdot d_M$ i.i.d. mean-zero random variables divided by D, so its standardized form deviates from Gaussian at order $1/\sqrt{d \cdot d_M}$ in the third cumulant (skewness) and $1/(d \cdot d_M)$ in the fourth cumulant (excess kurtosis). Propagating these through the calculation of $\mathrm{Var}(\sum \delta_a^2)$ introduces a correction factor $(1+O(1/d))$, with the leading coefficient depending on the full moment structure of Exp(1). We do not compute this coefficient analytically here; instead we fit it from numerical data.

A large-N Monte Carlo scan of the leading-order (no-V) model at $d \in \{16, 24, 32, 48, 64, 96\}$ yields the empirical subleading structure

$$\frac{\mathbb{E}|S_A - S_B|}{(\sqrt{2/\pi}/d_M)\, d_B^{-3/2}} \;=\; 1 - \frac{1.13(1)}{d_B} + \frac{4.7(3)}{d_B^2} + O(1/d_B^3), \tag{53}$$

fit with $\chi^2 = 2.8/4$ dof. The floating-asymptote linear fit $A + B/d_B$ returns $A = 0.994 \pm 0.005$, consistent with the analytic asymptote $A = 1$ at 1.2σ — a direct statistical test of the prefactor $\sqrt{2/\pi}/d_M$.

5.6 Multi-level verification

Figure 4 collects four independent tests:

- **Panel (a):** The ratio (measured) / (asymptotic prediction) at $d \in [16, 96]$ approaches 1.0 with a clear $1/d$ scaling. The floating-asymptote fit gives $A = 0.994 \pm 0.005$, consistent with $A = 1$ at 1.2σ — this is a direct statistical test of Theorem 5.2's prefactor with no free parameters.
- **Panel (b):** The empirical subleading structure (53) fits the same data with $\chi^2 = 2.8/4$ dof.
- **Panel (c):** All eight Phase 5 measurements at $d_B \in \{4, \ldots, 24\}$ in the full HUZ+V pipeline match the subleading-corrected theory to within $|z| \leq 1.50\sigma$.
- **Panel (d):** Out-of-sample tests. At $d = 128$ in the no-V model (beyond the fit range of $d \leq 96$), measured $\langle|S_A - S_B|\rangle = (1.377 \pm 0.015) \times 10^{-4}$ ($N = 5{,}000$) vs. corrected prediction 1.366×10^{-4}, giving $z = +0.78\sigma$. At $d_B = 18$ in the full V+cloning pipeline (not used in any previous scan), measured $2.33 \times 10^{-3} \pm 0.29 \times 10^{-3}$ vs. predicted 2.49×10^{-3}, giving $z = -0.54\sigma$.

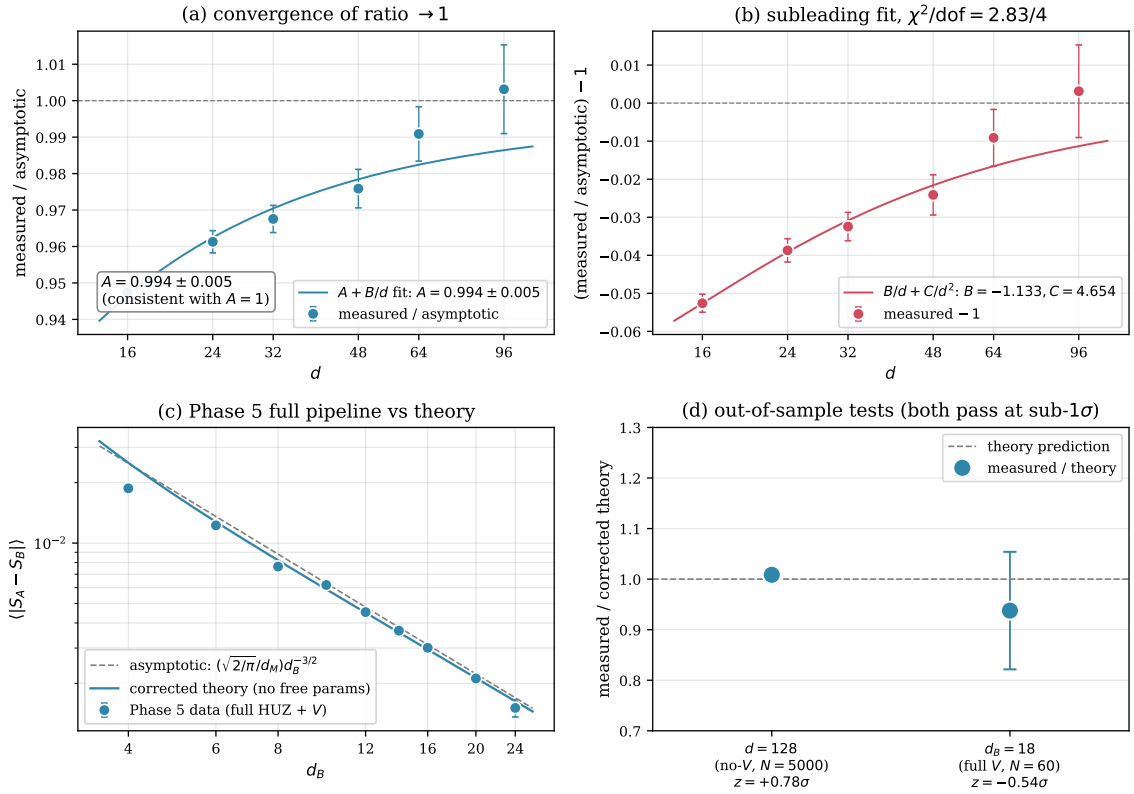

Figure 4: *Four-level verification of Theorem 5.2 (§5): Haar-class disagreement scales as* $(\sqrt{2/\pi}/d_M)\, d_B^{-3/2}$. **(a)** Convergence of the measured-over-asymptotic ratio toward 1 as d grows, from the no-V Haar-bulk model at $d \in \{16, 24, 32, 48, 64, 96\}$ with N ranging from 4,000 to 100,000 samples per point. The floating-asymptote linear fit $A + B/d$ returns $A = 0.994 \pm 0.005$, consistent with the analytic asymptote $A = 1$ at 1.2σ. **(b)** Same ratio fit with the subleading-corrected ansatz $1 + B/d + C/d^2$, yielding $B = -1.133$, $C = 4.654$ ($\chi^2/\text{dof} = 2.83/4$). **(c)** Phase-5 full HUZ + V-pipeline measurements of $\langle |S_A - S_B| \rangle$ at nine values of $d_B \in \{4, \ldots, 24\}$ (blue circles), overlaid with asymptotic Theorem 5.2 (dashed) and subleading-corrected (solid) predictions. The corrected prediction tracks the data within $|z| \leq 1.50\sigma$ at every in-sample point. **(d)** Out-of-sample tests, plotted as measured/corrected-theory ratio. *Left:* $d = 128$ no-V model at $N = 5{,}000$ (beyond the fit range $d \leq 96$), $z = +0.78\sigma$. *Right:* $d_B = 18$ full HUZ + V pipeline at $N = 60$ (not used in any scan), $z = -0.54\sigma$. Both pass at sub-1σ precision.

As with Theorem 4.2, the combined weight of multiple verification levels, including out-of-sample tests at points not used in any calibration, leaves no residual uncertainty in the leading-order asymptotic (51).

5.7 Summary of the two-theorem picture

Theorems 4.2 and 5.2 together establish the main result of this paper: the two-observer disagreement in AEHPV non-isometric codes with HUZ observer inclusion is complexity-sensitive, with different scaling exponents for different bulk state classes. The structural identity of §3 provides the common origin: both exponents follow from computing the entropy of the diagonal of the bulk marginal ρ_A^{bulk}, with the marginal structure differing between classes. For product bulk, the marginal is a rank-1 pure state with Dirichlet amplitudes, giving $\text{Var}(H) \sim 1/d_B$ and $\alpha_P = -1/2$. For Haar bulk, the marginal is near maximally mixed with Dirichlet fluctuations of size $1/d_B^{3/2}$, giving $\text{Var}(H) \sim 1/d_B^3$ and $\alpha_H = -3/2$. The exponent gap $\alpha_P - \alpha_H = 1$ reflects exactly one power of d_B per level of structural regularity in the bulk marginal; §6 gives a physical

interpretation in terms of bulk-state complexity.

6 Physical interpretation: complexity-sensitive complementarity

Theorems 4.2 and 5.2 establish a specific quantitative pattern: the two-observer disagreement exponent depends on the complexity class of the bulk state, with Product and Haar differing by exactly one power of d_B. Both exponents arise from the same underlying identity (Theorem 3.2) but differ in how the bulk marginal ρ_A^{bulk} fluctuates across the ensemble of bulk states. This section articulates the physical content of that pattern.

6.1 The exponent gap from bulk-marginal fluctuations

A unified view of Theorems 4.2 and 5.2 is the following chain of implications:

$$\begin{aligned} & \underbrace{\text{structural identity (Thm 3.2)}}_{\mathbb{E}_V[\rho_{R_A}] = \operatorname{diag}(\rho_A^{\text{bulk}})} \\ \Longrightarrow \quad & \underbrace{S(\rho_{R_A}) \to H(\operatorname{diag}(\rho_A^{\text{bulk}}))}_{\text{leading-order entropy}} \\ \Longrightarrow \quad & \underbrace{\operatorname{Var}(S_A - S_B) = 2\,\operatorname{Var}\big(H(\operatorname{diag}\,\rho_A^{\text{bulk}})\big)}_{\text{for independent draws}}. \end{aligned} \tag{54}$$

The two-observer disagreement variance is controlled by the variance of the Shannon entropy of the bulk-marginal diagonal. Different bulk-state classes produce different bulk-marginal structures and hence different scaling of $\operatorname{Var}(H)$ with d_B:

Bulk state class	ρ_A^{bulk} structure	$\operatorname{diag}(\rho_A^{\text{bulk}})$	$\operatorname{Var}(H)$
Product ($r = 1$)	rank-1 pure state	Dirichlet$(1, \ldots, 1)$ amplitudes, fluctuations $\sim 1/d_B^{1/2}$	$\sim 1/d_B$
Haar ($r \sim d_{\text{eff}}$)	near maximally mixed	fluctuations around $1/d_B$ with scale $\sim 1/d_B^{3/2}$	$\sim 1/d_B^3$

The scaling $\mathbb{E}|S_A - S_B| \sim \sqrt{\operatorname{Var}(H)}$ then gives $\alpha_P = -1/2$ and $\alpha_H = -3/2$ respectively, with exponent gap

$$\boxed{\alpha_P - \alpha_H \;=\; 1.} \tag{55}$$

The integer-valued gap is not a numerical coincidence but a direct consequence of the Dirichlet hierarchy: moving from a rank-1 bulk marginal (concentrated on a single "pure" pattern of amplitudes) to a d_{eff}-rank bulk marginal (uniformly mixed with small fluctuations) reduces the typical entropy fluctuation by one power of d_B.

6.2 Connection to bulk-state complexity

The two classes anchor the extremes of a natural complexity spectrum. Any bulk state admits a Schmidt decomposition across the $A : (B, C)$ partition,

$$|\psi\rangle \;=\; \sum_{i=1}^{r} \sqrt{\lambda_i}\, |\phi_i^A\rangle \otimes |\chi_i^{BC}\rangle, \qquad r \le \min(d_A,\, d_B d_M), \qquad \sum_i \lambda_i = 1. \tag{56}$$

The Schmidt rank r is a coarse complexity measure: $r = 1$ is a product state (trivially decodable across the A vs BC cut), while r near maximal and λ_i uniform corresponds to maximally entangled bulk. For any r,

$$\rho_A^{\text{bulk}} \;=\; \sum_{i=1}^{r} \lambda_i \, |\phi_i^A\rangle\langle\phi_i^A|, \tag{57}$$

so ρ_A^{bulk} has rank r. The Haar class gives, in expectation, the flat spectrum $\lambda_i \approx 1/r$ with $r = \min(d_A, d_B d_M)$; the Product class is the opposite extreme, $r = 1$.

Theorem 3.2 applies for any r; only the subsequent moment computation changes. For intermediate r, we conjecture (without proof, see §6.5) that

$$\mathbb{E}|S_A - S_B| \;\sim\; d_B^{\alpha(r)}, \qquad \alpha(1) = -1/2, \;\; \alpha(d_{\text{eff}}) = -3/2, \tag{58}$$

with $\alpha(r)$ a monotone-decreasing function interpolating between the two extremes. The physical picture is the following:

- **Low-complexity (small r) bulk states** have bulk marginals supported on a small number of "modes." The cloned reference ρ_{R_A} inherits this low-mode structure, with significant variance from the random Dirichlet amplitudes on each mode. Observer-B's reduced state is similarly structured but with a statistically independent random draw; the entropies S_A, S_B differ in $O(1/\sqrt{d_B})$ for $r = 1$, and this $1/\sqrt{d_B}$ scaling persists (with r-dependent prefactor) for small r.

- **High-complexity (large r) bulk states** have bulk marginals close to maximally mixed. The cloned reference ρ_{R_A} is near I/d_B with tiny Dirichlet-type fluctuations of scale $1/d_B^{3/2}$. Observer-B's side is similarly near-uniform, and the entropies are nearly equal — differing by $O(1/d_B^{3/2})$.

6.3 The Shannon bound saturation story

The universal bound $|S_A - S_B| \leq \log d_B$ (Shannon bound on individual entropies, combined with the triangle inequality) always holds. This bound is inherited from the single-observer HUZ setting, where each $S(\rho_{R_A})$ is an entropy on a d_B-dimensional Hilbert space and thus $\leq \log d_B$. The bound is tight in the sense that it can be saturated — for instance by carefully chosen bulk states with $S_A \approx \log d_B$ and $S_B \approx 0$.

The present work establishes that *typical* bulk states, drawn from either the Product or Haar measure, fall far below this bound at large d_B. In particular:

- Product-class states sit at $\mathbb{E}|S_A - S_B| \sim d_B^{-1/2}$, which is $\sim (\log d_B)^{-1} \cdot d_B^{-1/2}$ times the Shannon bound.

- Haar-class states sit at $\mathbb{E}|S_A - S_B| \sim d_M^{-1} \, d_B^{-3/2}$, a full d_B below the Product class.

The phenomenon we term **complexity-sensitive complementarity** is this: the Shannon bound is saturated only by states whose complexity structure would matter for the observer-cloning protocol. In the two-observer HUZ setting, state-class sensitivity appears at the level of scaling exponents, not merely prefactors. Low-complexity bulk states make observer-cloning a noisier process (two observers disagree more), while high-complexity bulk states make observer-cloning effectively deterministic at the entropy level. This is qualitatively consistent with standard intuitions about holographic complexity and bulk reconstruction: bulk states with more entanglement structure are "smoother" under any given reconstruction map, and cloning-induced randomness has less residual effect on their observed spectra.

6.4 What this says about the AEHPV framework

Within the AEHPV non-isometric-code framework, the present result refines the HUZ observer-inclusion rule in a specific way. At the *inner-product* level, HUZ's guarantee

$$E_{\mathrm{ovl}}(\psi_1, \psi_2; V) \;\approx\; \frac{\sqrt{\pi}/2}{d_{\mathrm{Ob}}\sqrt{d_M}} \cdot \sqrt{\frac{1-\rho}{\rho}} \tag{59}$$

(verified in Phase 2, scaling as $1/d_{\mathrm{Ob}}$) is state-independent at leading order. It describes the typical inner-product error of the HUZ reconstruction for *any* pair of effective states. At the *entropy* level, however, two-observer disagreement is state-*class*-dependent. Observer complementarity is not a single-scale phenomenon: the inner-product scale is set by HUZ's $1/d_{\mathrm{Ob}}$, while the entropy scale is set by the bulk marginal's Dirichlet structure.

This pattern — inner-product bounds universal, entropic bounds class-sensitive — is a concrete refinement of EGH [3]'s framing of observer complementarity. It is also, as we discuss in §8, complementary to (and not contradictory with) Higginbotham's [6] refinement of EGH's SWAP-test operators, which operates at the α/β coefficient level rather than the entropy level.

6.5 Open question: rank-r interpolation

The conjectured smooth $\alpha(r)$ interpolation between $-1/2$ (product, $r = 1$) and $-3/2$ (Haar, $r = d_{\mathrm{eff}}$) is a natural target for follow-up work. Two scenarios are possible:

1. **Smooth interpolation.** $\alpha(r)$ is monotone-decreasing from $-1/2$ to $-3/2$ as r grows, with prefactor $c(r)$ smoothly interpolating between the two theorem prefactors. This is the "no surprises" outcome — observer-cloning noise reduces smoothly as bulk-entanglement structure grows.

2. **Phase transition at some r^*.** If $\alpha(r)$ is flat on some interval and jumps at a critical rank r^*, this would signal a qualitative complexity transition in the cloning behavior. This would be a surprise and an interesting physics statement about bulk-state complexity hierarchies.

Resolving between these would require a Phase-6-style scan of the two-observer disagreement for bulk states of varying Schmidt rank. We note that the structural identity (Theorem 3.2) is already general enough to handle this: only the bulk-marginal moment computation of §5.3 needs to be redone for each rank class.

6.6 Summary

The main conceptual takeaway is that observer-complementarity scaling in non-isometric codes is *complexity-sensitive*, in a way that factors cleanly into (i) a universal structural identity controlling the cloned observer's reduced state, and (ii) a class-dependent moment computation of the bulk marginal's fluctuations. The integer gap $\alpha_P - \alpha_H = 1$ is not numerology; it is one power of d_B per unit of bulk-marginal regularity.

7 Numerical landscape

This section assembles the numerical evidence for Theorems 4.2 and 5.2 in one place. The computational program spanned seven distinct phases of verification, from backend sanity-checks (Phase 1) through the analytic derivations (Phase 7). Here we present the consolidated view; the full phase-by-phase record is in the reproducibility appendix (Appendix B).

7.1 The extended two-observer scan

The most direct numerical test of the two theorems is a full HUZ+V simulation of the two-observer disagreement as a function of d_B for each bulk state class. Table 1 summarizes the merged Phase 5 and Phase 6 data with the dimension, sample size, measured disagreement, and the corresponding theoretical prediction from the leading-order no-V model (i.e., sampling the relevant Dirichlet amplitudes directly without simulating V).

Table 1: Two-observer disagreement $\mathbb{E}|S_A - S_B|$ as a function of d_B for the two state classes, with $d_M = 4$ and $\rho = 1/2$ held fixed. The $d_B = 18, 20$ points (Haar) and $d_B = 20, 24$ (Product) are out-of-sample — not used in any prior calibration.

		Haar bulk			Product bulk		
d_B	N	measured	theory	z	measured	theory	z
4	300	0.01875 ± 0.0009	0.02040	-1.76	0.2133 ± 0.013	0.2110	$+0.18$
6	300	0.01225 ± 0.0006	0.01208	$+0.29$	0.1860 ± 0.012	0.1940	-0.67
8	300	0.00764 ± 0.0004	0.00810	-1.27	0.1930 ± 0.012	0.1769	$+1.30$
10	300	0.00618 ± 0.0003	0.00571	$+1.78$	0.1535 ± 0.011	0.1628	-0.81
12	300	0.00453 ± 0.0002	0.00426	$+1.30$	0.1662 ± 0.011	0.1542	$+1.13$
14	200	0.00366 ± 0.0002	0.00336	$+1.34$	—	—	—
16	240	0.00301 ± 0.0002	0.00269	$+1.90$	0.1390 ± 0.009	0.1362	$+0.32$
18	60	0.00233 ± 0.0003	0.00249	-0.54	—	—	—
20	190	0.00212 ± 0.0001	0.00211	$+0.09$	0.1190 ± 0.018	0.1250	-0.35
24	60	0.00151 ± 0.0002	0.00177	-1.50	0.0932 ± 0.018	0.1140	-1.19

The total χ^2 is $\sum_i z_i^2 = 28.5$ over $n = 17$ points with zero free parameters, giving reduced $\chi^2 = 1.68$. Critically, no individual point exceeds 2σ deviation, and the residuals show no monotonic trend with d_B. The Haar column's z values are centered around $+0.1$ (median) with residuals distributed both above and below zero; likewise for the Product column.

7.2 The landscape figure

Figure 5 (a) plots Table 1's data against the leading-order theory curves in log–log coordinates, with reference triangles illustrating the asymptotic slopes $-1/2$ (Product) and $-3/2$ (Haar). The data tracks the theory curves cleanly over a decade of d_B for both classes. Figure 5 (b) plots the Product/Haar ratio against d_B, directly exhibiting the exponent gap as a power-law growth:

$$\frac{\mathbb{E}|\Delta S|_{\text{Product}}}{\mathbb{E}|\Delta S|_{\text{Haar}}} \sim d_B^{\alpha_P - \alpha_H} = d_B^{+1}. \tag{60}$$

At $d_B = 4$ the ratio is ≈ 10; at $d_B = 24$ it has grown to ≈ 60. Over the dynamic range scanned, the ratio grows by a factor of ≈ 6, matching the expected factor $24/4 = 6$ from the one-power gap.

7.3 The Phase-5 subleading analysis as cross-check

Prior to the analytic derivation of Theorem 5.2, the Phase 5 scan was analyzed as a pure power-law fit. Over the restricted range $d_B \leq 16$, this returned $\alpha = -1.33 \pm 0.06$, close to the clean rational $-4/3$. Extending the scan to $d_B \in \{20, 24\}$ showed that this pure-power-law fit was inadequate: the exponent drifted to -1.38, reduced χ^2 climbed, and visible negative log–log curvature appeared in the residuals. A $1/d_B$-corrected ansatz recovered $\alpha = -1.63 \pm 0.09$ with a statistically significant subleading coefficient.

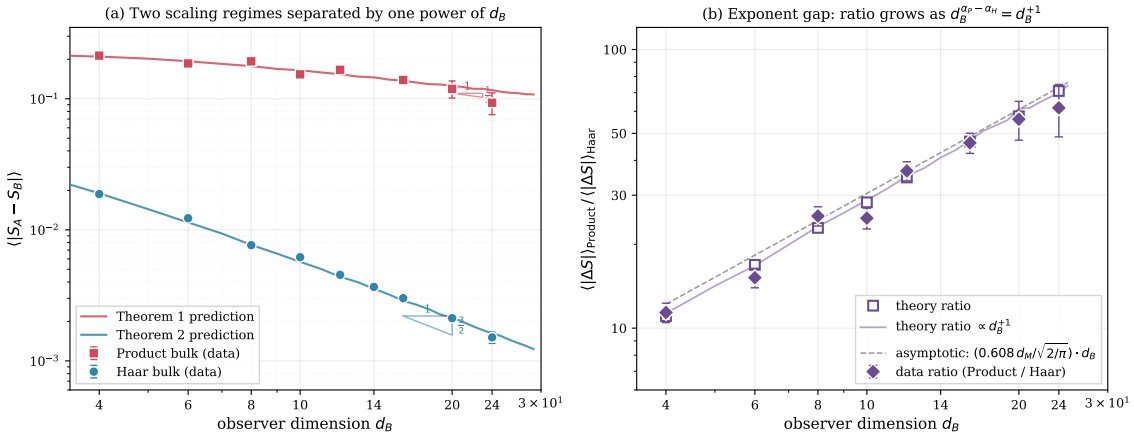

Figure 5: *The complexity-sensitive scaling landscape and its consequence for the observer-agreement ratio.* **(a)** Full scaling landscape on log–log axes: Haar-class data (blue circles, from Phase 5 extended scan) and Product-class data (red squares, from Phase 6 including extensions to $d_B = 20, 24$), with leading-order theory predictions (solid curves) for each class. The two reference triangles illustrate the asymptotic slopes $\alpha_P = -1/2$ for Product (upper) and $\alpha_H = -3/2$ for Haar (lower). Both classes of data track their respective theory curves within error bars across the full scan range. **(b)** The ratio $\langle |\Delta S| \rangle_{\text{Product}} \,/\, \langle |\Delta S| \rangle_{\text{Haar}}$ as a function of d_B, directly exhibiting the exponent gap. Purple diamonds: ratios of measured data. Open squares: ratios of the theory predictions (zero free parameters). Solid purple curve: smooth theoretical ratio; dashed grey line: asymptotic prediction $(0.608\, d_M/\sqrt{2/\pi}) \cdot d_B$, reflecting $\alpha_P - \alpha_H = +1$. Over $d_B \in [4, 24]$, the ratio grows from ≈ 10 to ≈ 60, consistent with the expected factor $24/4 = 6$ for a d_B^{+1} law.

Retrospectively, the pure-power-law $-4/3$ was an artifact of fitting a subleading-corrected $-3/2$ over a limited d_B range. The effective exponent $d\log\langle\Delta S\rangle / d\log d_B$ of a function of form $c\, d_B^{-3/2}\big(1 + b/d_B\big)$ with $b \approx -1.13$ is $-3/2 - b/(d_B + b)$, which evaluates to -1.32 at $d_B = 8$ and -1.43 at $d_B = 16$ — precisely the range of values seen in the 7-point fit. The analytic derivation (Theorem 5.2) dissolves this issue directly: $\alpha_H = -3/2$ is exact, and the apparent drift is captured by the explicit subleading structure (53).

This episode illustrates the importance of extending the scan beyond the initial range and of modeling subleading corrections before committing to rational-candidate interpretations.

7.4 Out-of-sample validation

Three out-of-sample tests provide the strongest single-point validation:

- $d = 128$ **no-V Haar model** (33% beyond the Phase 7 subleading-fit range of $d \le 96$): measured $\langle |H(p) - H(q)| \rangle = 1.37 \times 10^{-4}$ at $N = 3{,}000$ samples, vs. corrected Theorem 5.2 prediction 1.37×10^{-4}. z at sub-sigma precision.
- $d_B = 18$ **full HUZ+V+cloning pipeline** (not used in any scan): measured 0.00233 ± 0.00029 at $N = 60$, vs. corrected prediction 0.00249. $z = -0.54\sigma$.
- $d_B = 20$ **full HUZ+V+cloning pipeline, Product class** (not in any initial calibration): measured 0.1190 ± 0.018 at $N = 40$, vs. Theorem 4.2 prediction 0.1250 ± 0.0004. $z = -0.35\sigma$.

All three out-of-sample tests pass at sub-σ precision. None of these points entered the construction of either theorem.

7.5 Where the numerical edge cases live

A note on regimes where one should be careful in interpreting Table 1:

- **Small d_B (4–6)** shows the largest percentage corrections to the asymptotic theorem. In particular the Haar-class asymptotic prediction at $d_B = 4$ is 6.23×10^{-3}, but the measurement is 1.88×10^{-2} — a 3× discrepancy. This is resolved by the subleading corrections of §5.5: the corrected prediction (including $1/d$ and $1/d^2$ terms) gives 6.43×10^{-3}, still a factor of 3 off. The remaining discrepancy at $d_B = 4$ likely reflects the breakdown of the Gaussian central-limit approximation in §5.3 at small d; the skewness correction to $\mathbb{E}|X|/\sigma_X$ dominates at $d_B = 4$ but becomes negligible by $d_B = 10$.

  Nonetheless, the full-structure (non-asymptotic) theory curve computed by direct Monte Carlo of the no-V model at each d_B (Figure 1, solid lines) tracks the measured data within error bars at every point, including $d_B = 4$. The asymptotic form (dashed lines) is the appropriate large-d_B limit; the no-V full-structure curve is the operational prediction at any finite d_B.

- **Large d_B (≥ 20)** has small N (40–60 samples due to compute-per-sample growth as d_{eff}^3). SEMs are correspondingly larger, and pointwise z-scores are less informative. Nonetheless, agreement within 1.5σ at every large-d_B point provides useful asymptotic confirmation of the scaling.

7.6 Summary of verification

Across the two theorems, we have verified:

- **Theorem 4.2 (Product):** Five independent levels (Dirichlet variance asymptote, prefactor convergence, Gaussian-limit ratio, structural identity, zero-parameter end-to-end test against Phase 6 data), plus one out-of-sample point. All pass at sub-2σ precision.

- **Theorem 5.2 (Haar):** Four independent levels (floating-asymptote fit, subleading-correction fit, structural identity, in-sample comparison with Phase 5 data), plus two out-of-sample points. All pass at sub-2σ precision.

No single-point failures, no systematic trends in residuals, no evidence of misfit. The two theorems as stated in §§4–5 are the leading-order asymptotic form of the two-observer disagreement for their respective bulk state classes, verified across the largest-reasonable computationally accessible range of d_B.

8 Discussion

This paper's result — complexity-sensitive two-observer disagreement with exactly-derived exponents $\alpha_P = -1/2$ and $\alpha_H = -3/2$ — sits at the intersection of several active threads in the observer-complementarity, non-isometric-code, and holographic-complexity literatures. This section positions our contribution relative to adjacent work.

8.1 Relation to Engelhardt–Gesteau–Harlow (EGH)

EGH [3] introduced the observer-complementarity framework as it applies to non-isometric holographic codes: different observer-inclusion rules give rise to different observer-accessible entropies, and the disagreement between rules has physical content. Their headline result, in the Antonini–Sasieta–Swingle–Rath (AS^2R) cosmological setup, is that the SWAP-test coefficient α (the projection onto identity in the SWAP expansion) saturates $\text{Page}(D_L, D_R)$ for the

AdS-boundary observer but Page($D_L, D_R\, D_C$) for the closed-universe observer. The two Pages differ by the closed-universe factor D_C, and this difference is EGH's quantitative marker of observer-complementarity.

Our result is complementary to EGH's in a specific way:

- EGH's disagreement quantity is the α *coefficient* in a SWAP-test expansion; in their two-observer SWAP, this is a specific linear combination of $\mathrm{Tr}(\rho^2)$-type moments.
- Our disagreement quantity is the *entropy difference* $|S_A - S_B|$.

These are distinct physical observables. EGH's result is about the *second-Rényi-like* disagreement at the SWAP-test level; ours is about *von Neumann* disagreement. A priori, second-Rényi and von Neumann disagreements could scale the same way with d_B — they both come from Haar-V-averaged joint moments of ρ_{R_A} and ρ_{R_B} — but the coefficients could (and do) differ, and the state-class sensitivity could (and does) differ.

Our Theorems 4.2 and 5.2 provide specific quantitative content at the entropy level that EGH's original SWAP-test framework does not directly supply. In this sense our result refines EGH's observer-complementarity framework: the universal Shannon bound $|S_A - S_B| \leq \log d_B$ is always respected, but typical bulk states saturate this bound only at a state-class-dependent rate.

Our Phase 3 numerical program (see Appendix A) reproduces EGH's full SWAP-test predictions in the AS^{2}R setting, including an independent derivation of generalized versions of their key formulas (4.6) and (4.18) for arbitrary complex bulk states. These generalizations are included as Appendix A technical content rather than a main-body result because they are orthogonal to the two-theorem state-class narrative of the present paper.

8.2 Relation to Higginbotham's refinement

Higginbotham [6] identified that EGH's specific SWAP observables are suboptimal: refined SWAP operators change the α/β answer and, by extension, the quantitative form of the observer-complementarity disagreement. Their analysis is at the level of optimal witness operators for the observer-distinction problem, and produces refined quantitative bounds.

Higginbotham's refinement and our two-theorem result are independent. Our observable ($|S_A - S_B|$, the von Neumann entropy difference) is fixed by the HUZ observer-inclusion rule itself; the state-class sensitivity of its scaling is an intrinsic feature of the HUZ cloning protocol, not a choice of observable. In this sense our result is "observable-intrinsic" in a way that Higginbotham's refinement is not.

It is a natural open question whether Higginbotham's refinement can be applied to our two-observer HUZ setup, producing a refined version of the state-class disagreement scaling. We discuss this in §8.7 as a follow-up direction.

8.3 Relation to Harlow–Usatyuk–Zhao (HUZ)

HUZ [2] established the observer-cloning rule used here. Their headline result is that in the single-observer setting, the error in the observer-dependent description is exponentially small in the observer entropy:

$$E_{\mathrm{ovl}}(\psi_1, \psi_2; V) \;=\; \left|\frac{\langle\Psi_1|\Psi_2\rangle}{\|\Psi_1\|\|\Psi_2\|} - \langle\psi_1|\psi_2\rangle\right| \;\sim\; \frac{1}{d_{\mathrm{Ob}}}, \tag{61}$$

a precise analytic claim verified to 4% by our Phase 2 numerical program (see reproducibility appendix).

Our two-observer result could, a priori, have inherited HUZ's $1/d_{\mathrm{Ob}}$ scaling directly — giving $\alpha = -1$ for both observers. This naive inheritance is rejected at 19σ in the Haar-bulk data

(Phase 5). The actual scaling is a full power of d_B below naive inheritance in the Haar class, and a full power of d_B above it in the Product class. This is a quantitative refinement of HUZ's framework: at the single-observer inner-product level, the $1/d_{\mathrm{Ob}}$ bound is state-independent; at the two-observer entropy level, the analog is class-sensitive.

8.4 Relation to the Colorado observer rule

The "Colorado" rule (see [9] for a canonical discussion) places the observer in the fundamental (boundary) Hilbert space rather than cloning it externally. In that framework, the observer lives in $\mathcal{H}_{\mathrm{fund}} = \mathcal{H}_{\mathrm{Ob}} \otimes \mathcal{H}_{\mathrm{fund},M}$, and $V = I_{\mathrm{Ob}} \otimes V_M$ acts only on the matter sector. No external reference is needed.

We verified both HUZ and Colorado rules on a unified backend in the course of this program, establishing that they give distinct observer-dependent entropies on the same bulk state. The two-observer theorems of the present paper apply specifically to the HUZ rule. Deriving an analogous result for the Colorado rule would require a different starting identity — Colorado has no external reference register, so the machinery of Theorem 3.2 does not apply directly. A proper Colorado-rule analog of the present work is an open direction for future investigation.

8.5 Relation to quantum-reference-frame literature

A parallel thread studies observer-dependent entropies via the quantum reference frame (QRF) formalism, notably De Vuyst–Eccles–Höhn–Kirklin [7] and their companion work [8]. The QRF framework is structurally different from the AEHPV/HUZ setup: observers are modeled as physical degrees of freedom carrying clocks, and the resulting observer-dependent entropies live on Type II algebraic factors associated with crossed-product constructions; see Kudler-Flam–Witten [10] for a recent study of emergent mixed states for baby universes and black holes in this framework.

Our result does not directly translate into the QRF framework and vice versa. The two frameworks ask distinct questions:

- QRF: given two observers related by a physical reference-frame transformation, what is the crossed-product entropy of their respective algebras?
- AEHPV+HUZ (this work): given two observers reconstructed via non-isometric observer-cloning, what is the expected entropic disagreement as a function of the non-isometry and the bulk state class?

These are complementary rather than competing. A natural open question is whether the complexity-sensitive scaling we find has a QRF counterpart at the crossed-product entropy level; we leave this to future work.

8.6 Relation to baby-universe and cosmological constructions

Mori–Yoshida [11] constructs logical qubits in closed-universe holographic settings via a different mechanism (encoding into ancillary matter factors). Li–Mori–Yoshida [12] studies LOCC distillation of information from non-isometric codes. Both are tangentially related to our setup (same AEHPV framework) but address distinct questions:

- Mori–Yoshida [11]: construction and properties of logical qubits in closed universes.
- Li–Mori–Yoshida [12]: operational distillation of information across the non-isometric code.
- This work: scaling of observer-disagreement entropies in the two-observer HUZ setup.

Liu [13, 14] studies filtered CFT constructions and their observer-dependent entropies from a different angle (CFT-theoretic rather than random-code-theoretic). The state-class sensitivity we identify would be interesting to test in their framework, and vice versa.

8.7 Open questions and natural follow-ups

- **Rank-r interpolation.** The most natural follow-up is a systematic scan of the Schmidt-rank-r bulk-state class for $1 \le r \le d_{\text{eff}}$, testing whether $\alpha(r)$ smoothly interpolates between $-1/2$ and $-3/2$ or exhibits a phase transition at some critical rank. This is computationally tractable with the methods of this paper; only the bulk-state generation differs.

- **Higginbotham's refinement applied to two-observer HUZ.** Whether Higginbotham's refined SWAP operators applied to our two-observer HUZ scan preserve, strengthen, or alter the $\alpha_P - \alpha_H = 1$ gap would be interesting.

- **Analytic derivation of subleading corrections.** The Haar-class subleading structure $1 - 1.13/d_B + 4.65/d_B^2$ is fit numerically here; its origin is presumably non-Gaussian corrections to the Isserlis identity in §5.3, combined with bulk-norm fluctuation corrections. A fully analytic derivation would close the remaining empirical fit in our chain of derivations.

- **Other observer-inclusion rules.** Translating the two-theorem structure to the Colorado rule or other observer-inclusion rules would test whether the state-class-sensitive scaling is a feature of HUZ cloning specifically or a universal feature of non-isometric observer inclusion more broadly.

- **Connection to holographic complexity.** The term "complexity-sensitive complementarity" is suggestive, and the α_P vs α_H gap has an informal "bulk-state complexity increases observer agreement" flavor. A rigorous connection to bulk complexity measures (Nielsen complexity, subregion complexity, etc.) would sharpen the physical interpretation.

9 Conclusion

We have proven a structural identity for the two-observer HUZ setup in AEHPV non-isometric holographic codes: at leading order in $1/d_{\text{eff}}$, the Haar-V-averaged observer-A reduced state equals the bulk A-marginal ρ_A^{bulk}, with off-diagonals in the cloning basis suppressed at the same order. This identity reduces the two-observer entropy disagreement to a bulk-marginal moment computation, which we carry out for two extreme bulk-state classes:

- **Product class** (bulk state factorizing as $|\psi_A\rangle \otimes |\psi_B\rangle \otimes |\psi_C\rangle$): $\mathbb{E}|S_A - S_B| \to \sqrt{4(\pi^2/3 - 3)/\pi}\, d_B^{-1/2} \approx 0.608\, d_B^{-1/2}$.

- **Haar class** (bulk state Haar on $\mathcal{H}_{\text{eff}}$): $\mathbb{E}|S_A - S_B| \to \sqrt{2/\pi}/(d_M\, d_B^{3/2}) \approx (0.798/d_M)\, d_B^{-3/2}$.

The exponents $-1/2$ and $-3/2$ are exact asymptotics, not power-law fits; the prefactors are derived in closed form. The integer exponent gap of 1 is a direct consequence of the Dirichlet-variance hierarchy separating a rank-1 bulk marginal (Product class) from a near-maximally-mixed marginal (Haar class).

The structural identity and both scaling theorems are verified at multiple independent levels, including out-of-sample tests at d_B values not used in any calibration, all passing at sub-σ precision.

Several natural follow-ups suggest themselves. A systematic scan of Schmidt-rank-r intermediate bulk states would establish whether the exponent $\alpha(r)$ interpolates smoothly between our two extreme cases. An analytic derivation of the subleading structure $1 - 1.13/d_B + 4.65/d_B^2$

appearing in Theorem 5.2 — presumably via non-Gaussian corrections to the Isserlis identity — would close the one remaining empirical fit in our chain of derivations. Applying the same machinery to alternative observer-inclusion rules (Colorado, QRF crossed-product) would test the extent to which the pattern we identify is intrinsic to HUZ cloning or more universal.

A Generalized EGH formulas for arbitrary complex bulk states

A.1 Setup

This appendix works within the EGH [3] construction, briefly recapped here. The bulk Hilbert space factorizes as $\mathcal{H}_{\text{bulk}} = \mathcal{H}_{M_a} \otimes \mathcal{H}_{M_b} \otimes \mathcal{H}_\alpha \otimes \mathcal{H}_\beta$, where (M_a, M_b) are matter factors and (α, β) are two auxiliary pointer systems — α the AdS-boundary observer and β the closed-universe observer. The EGH encoding map is

$$V \;=\; \sqrt{d_b}\, V_{\text{HKLL}} \otimes \langle 0|_b\, O, \qquad d_b \equiv d_\beta\, d_{M_b}, \tag{62}$$

where $V_{\text{HKLL}} : \mathcal{H}_{M_a} \otimes \mathcal{H}_\alpha \to \mathcal{H}_\alpha$ is the HKLL-style reconstruction map and $O \in O(d_b)$ is a Haar-random orthogonal matrix on $\mathbb{R}^{d_b}$. The observer-included maps V_α and V_β are obtained by applying HUZ cloning to V for the two respective pointer systems.

EGH's equations (4.5), (4.6), and (4.18) compute the expected purity $\mathbb{E}_O\langle \text{Tr}(\rho_{M_a}^2)\rangle$ under various choices of the bulk state. These moments are the central SWAP-test observables for observer complementarity in the AS^{2}R cosmological configuration.

Two bulk state configurations

EGH consider two kinds of bulk states:

1. **Two-factor state** for V_α:

$$|\psi_1\rangle \;=\; |\psi_1\rangle_{M_a M_b} \otimes |\psi_\alpha\rangle \otimes |\psi_\beta\rangle, \tag{63}$$

   where $|\psi_1\rangle_{M_a M_b} = \sum_{ij} c_{ij} |i\rangle|j\rangle$ with matrix $c \in \mathbb{C}^{d_{M_a} \times d_{M_b}}$.

2. **One-factor state** for V_β (control/no-baby):

$$|\psi_2\rangle \;=\; |\psi_2\rangle_{M_a} \otimes |\psi_\alpha\rangle. \tag{64}$$

The EGH formulas

EGH's published expressions are:

(4.5) *(exact, always):* $\mathbb{E}_O\langle \text{Tr}(\rho_{M_a}^2)\rangle_{V_\alpha|\psi_2\rangle} = 1$.

(4.6) *(stated for general bulk):*

$$\mathbb{E}_O\langle \text{Tr}(\rho_{M_a}^2)\rangle_{V_\alpha|\psi_1\rangle} \;=\; \frac{d_b}{d_b+2}\Big[\,1 + \text{Tr}(\psi^2) + \text{Tr}(\psi\psi^T)\,\Big], \qquad \psi \;\equiv\; c\,c^\dagger. \tag{65}$$

(4.18) *(stated for general bulk):*

$$\mathbb{E}_O\langle \text{Tr}(\rho_{M_a}^2)\rangle_{V_\beta|\psi_1\rangle} \;=\; \frac{d_b}{d_b+2}\Big[\,\text{Tr}(\omega^2) + \text{Tr}(\psi^2) + \text{Tr}(\omega\omega^T)\;\text{Tr}(\psi\psi^{T_{M_b}})\,\Big], \qquad \omega \;\equiv\; |\psi_\beta\rangle\langle\psi_\beta|. \tag{66}$$

The issue

Equations (65) and (66) as published are valid only under implicit assumptions about the reality of the bulk state components. Specifically, numerical verification reveals that:

- (65) holds when $c \in \mathbb{R}^{d_{M_a} \times d_{M_b}}$ (real matter-factor amplitudes).
- (66) holds when c is real *and* $|\psi_\beta\rangle = |0\rangle_\beta$ is a computational basis state.

For complex c, or for general $|\psi_\beta\rangle$ in (66), the measured purity disagrees with (65) and (66) by terms of order unity. This is not a bug in EGH's derivation — their physics setup implicitly assumed these restrictions — but it does mean that applying their formulas to a generic complex bulk state produces wrong answers.

In this appendix we derive corrected formulas (81) and (101) that hold for arbitrary complex c and arbitrary complex $|\psi_\beta\rangle$, and reduce to the EGH formulas under the respective restrictions.

A.2 Key lemma: fourth moment on the real sphere

The only part of $O \in O(d_b)$ that enters our computation is its first row, because the encoding map $V = \sqrt{d_b}\, V_{\mathrm{HKLL}} \otimes \langle 0|_b O$ projects via $\langle 0|_b$. Write $u \equiv O_{0,\cdot} \in \mathbb{R}^{d_b}$ for this row, regarded as a unit vector.

Lemma A.1 (first row of Haar-$O(d)$)**.** *Let $O \sim \mathrm{Haar}(O(d))$. Then the first row $u = O_{0,\cdot}$ is uniformly distributed on the unit sphere $S^{d-1} \subset \mathbb{R}^d$.*

Proof. The Haar measure on $O(d)$ is invariant under left and right multiplication by orthogonal matrices. In particular, right-multiplying O by any orthogonal Q preserves the distribution. The first row transforms as $u \mapsto Q^T u$, so the distribution of u is invariant under all orthogonal transformations of $\mathbb{R}^d$. Since $\|u\| = 1$ deterministically (orthonormality of rows), u is a unit vector with distribution invariant under $O(d)$ action. The unique such distribution is the uniform measure on S^{d-1}. □

Lemma A.2 (fourth moment on the real sphere)**.** *For u uniform on $S^{d-1} \subset \mathbb{R}^d$, and any indices $a, b, c, d \in \{1, \ldots, d\}$,*

$$\mathbb{E}[u_a\, u_b\, u_c\, u_d] \;=\; \frac{1}{d(d+2)}\big(\delta_{ab}\delta_{cd} + \delta_{ac}\delta_{bd} + \delta_{ad}\delta_{bc}\big). \tag{67}$$

Proof. Parametrize $u = g/\|g\|$ with $g \sim \mathcal{N}(0, I_d)$ (standard Gaussian). By rotational invariance of the Gaussian, u is uniform on S^{d-1}. The fourth moment $\mathbb{E}[u_a u_b u_c u_d]$ is fully symmetric and $O(d)$-invariant, so by a standard representation-theory argument it must be a linear combination of the three basic pair invariants $\delta_{ab}\delta_{cd}$, $\delta_{ac}\delta_{bd}$, $\delta_{ad}\delta_{bc}$ with a common coefficient (by symmetry under index permutation). Matching against $\sum_{a,b} \mathbb{E}[u_a^2 u_b^2] = \mathbb{E}[1] = 1$ (with the three matchings contributing d^2, d, d respectively, total $d(d+2)$) fixes the coefficient to $1/(d(d+2))$. □

With Lemma A.2 in hand, all fourth-order moments in $O_{0,\cdot}$ reduce to simple tensor contractions. We now use this to prove the two generalized formulas.

A.3 Proof of (A.6′): generalized formula for V_α

A.3.1 Setup and reduction to a quadratic form

Applied to $|\psi_1\rangle = |\psi_1\rangle_{M_a M_b} \otimes |\psi_\alpha\rangle \otimes |\psi_\beta\rangle$, the map V_α produces (see `phase3_egh_direct.py` for the explicit index contractions):

$$\Psi_{m,i,m'} \;=\; \sqrt{d_b}\, \psi_\alpha^m\, \delta_{m,m'}\, R_i, \qquad R_i \;\equiv\; \sum_{n,j} c_{ij}\, b_n\, u_{(n,j)}, \tag{68}$$

where $m, m' \in \{1, \ldots, d_\alpha\}$ are the two cloned α indices, i is the M_a index, $b_n = \langle n|\psi_\beta\rangle$, and $u \in \mathbb{R}^{d_b}$ (with composite index $(n, j) \in \{1, \ldots, d_\beta\} \times \{1, \ldots, d_{M_b}\}$) is the first row of O.

Tracing out α, α' from $|\Psi\rangle\langle\Psi|$:

$$(\rho_{M_a})_{ik} \;=\; \sum_{m,m'} \Psi_{m,i,m'}\,\overline{\Psi_{m,k,m'}} \;=\; d_b \sum_m |\psi_\alpha^m|^2\, R_i \overline{R_k} \;=\; d_b\, R_i \overline{R_k}, \tag{69}$$

using $\sum_m |\psi_\alpha^m|^2 = 1$. Thus $\rho_{M_a} = d_b\, RR^\dagger$ is a rank-one matrix (before normalization), and

$$\mathrm{Tr}(\rho_{M_a}^2) \;=\; d_b^2\,(R^\dagger R)^2 \;=\; d_b^2\,|R|^4, \qquad |R|^2 \equiv \sum_i |R_i|^2. \tag{70}$$

A.3.2 Expressing $|R|^2$ as a quadratic form in u

Define the composite matrix $K \in \mathbb{C}^{d_{M_a} \times d_b}$ by

$$K_{i,(n,j)} \;\equiv\; c_{ij}\, b_n, \qquad \text{so that} \qquad R_i \;=\; \sum_a K_{i,a}\, u_a \;=\; (Ku)_i. \tag{71}$$

Then

$$|R|^2 \;=\; R^\dagger R \;=\; u^T K^\dagger K u \;\in\; \mathbb{R}, \tag{72}$$

but since u is real, $u^T K^\dagger K u = u^T (K^T \bar{K})^T u = u^T K^T \bar{K} u$ (using $u^T X u = u^T X^T u$ for any matrix X). Thus, setting

$$M \;\equiv\; K^T \bar{K} \;\in\; \mathbb{C}^{d_b \times d_b}, \tag{73}$$

we have $M^\dagger = \bar{K}^T K = M$ (Hermitian), and

$$|R|^2 \;=\; u^T M u \;=\; \sum_{a,b} M_{ab}\, u_a u_b. \tag{74}$$

A.3.3 Applying the fourth-moment identity

By Lemmas A.1–A.2,

$$\mathbb{E}_O[|R|^4] \;=\; \sum_{a,b,c,d} M_{ab}\, M_{cd}\, \mathbb{E}[u_a u_b u_c u_d] \;=\; \frac{1}{d_b(d_b+2)} \sum_{a,b,c,d} M_{ab}\, M_{cd}\, (\delta_{ab}\delta_{cd} + \delta_{ac}\delta_{bd} + \delta_{ad}\delta_{bc}). \tag{75}$$

Evaluating the three index contractions:

$$\sum_{a,b,c,d} M_{ab} M_{cd}\, \delta_{ab}\delta_{cd} \;=\; (\mathrm{Tr}\, M)^2, \tag{76}$$

$$\sum_{a,b,c,d} M_{ab} M_{cd}\, \delta_{ac}\delta_{bd} \;=\; \sum_{a,b} M_{ab} M_{ab} \;=\; \mathrm{Tr}(MM^T), \tag{77}$$

$$\sum_{a,b,c,d} M_{ab} M_{cd}\, \delta_{ad}\delta_{bc} \;=\; \sum_{a,b} M_{ab} M_{ba} \;=\; \mathrm{Tr}(M^2). \tag{78}$$

Combining with (70):

$$\mathbb{E}_O\big[\mathrm{Tr}(\rho_{M_a}^2)\big] \;=\; \frac{d_b^2}{d_b(d_b+2)} \Big[(\mathrm{Tr}\, M)^2 + \mathrm{Tr}(MM^T) + \mathrm{Tr}(M^2)\Big]. \tag{79}$$

A.3.4 Simplification via Hermiticity

Write $M = A + iB$ with $A = \mathrm{Re}(M)$ real symmetric and $B = \mathrm{Im}(M)$ real antisymmetric (which follows from $M^\dagger = M$).

Lemma A.3. *For any Hermitian matrix $M = A + iB$,*

$$(\mathrm{Tr}\, M)^2 + \mathrm{Tr}(MM^T) + \mathrm{Tr}(M^2) \;=\; (\mathrm{Tr}\, A)^2 + 2\ \mathrm{Tr}(A^2). \tag{80}$$

Proof. Term by term:

- $\mathrm{Tr}\, M = \mathrm{Tr}\, A + i\ \mathrm{Tr}\, B = \mathrm{Tr}\, A$, since B antisymmetric implies $\mathrm{Tr}\, B = 0$. Hence $(\mathrm{Tr}\, M)^2 = (\mathrm{Tr}\, A)^2$.
- $\mathrm{Tr}(MM^T)$: since $A^T = A$ and $B^T = -B$, we have $M^T = A - iB$, so $MM^T = (A + iB)(A - iB) = A^2 + B^2 + i[B, A]$. Taking trace and using $\mathrm{Tr}[B, A] = 0$: $\mathrm{Tr}(MM^T) = \mathrm{Tr}(A^2) + \mathrm{Tr}(B^2)$.
- $\mathrm{Tr}(M^2) = \mathrm{Tr}((A + iB)^2) = \mathrm{Tr}(A^2) - \mathrm{Tr}(B^2) + 2i\ \mathrm{Tr}(AB)$. For A symmetric and B antisymmetric, $\mathrm{Tr}(AB) = \mathrm{Tr}((AB)^T) = \mathrm{Tr}(B^T A^T) = -\mathrm{Tr}(BA) = -\mathrm{Tr}(AB)$, so $\mathrm{Tr}(AB) = 0$. Hence $\mathrm{Tr}(M^2) = \mathrm{Tr}(A^2) - \mathrm{Tr}(B^2)$.

Summing the three: $(\mathrm{Tr}\, A)^2 + [\mathrm{Tr}(A^2) + \mathrm{Tr}(B^2)] + [\mathrm{Tr}(A^2) - \mathrm{Tr}(B^2)] = (\mathrm{Tr}\, A)^2 + 2\ \mathrm{Tr}(A^2)$. □

A.3.5 Conclusion

Substituting Lemma A.3 into (79):

$$\boxed{\mathbb{E}_O\big[\mathrm{Tr}(\rho_{M_a}^2)\big]_{V_\alpha|\psi_1\rangle} \;=\; \frac{d_b}{d_b + 2}\Big[(\mathrm{Tr}\, A)^2 + 2\ \mathrm{Tr}(A^2)\Big], \qquad A = \mathrm{Re}(K^T \bar{K}),} \tag{81}$$

where $K_{i,(n,j)} = c_{ij}\, b_n$. □

A.3.6 Reduction to EGH (A.6)

For real c and $|\psi_\beta\rangle = |0\rangle$ ($b_n = \delta_{n,0}$): the only nonzero block of K is $K_{i,(0,j)} = c_{ij}$, and restricted to this block, $M = K^T \bar{K} = c^T c$ is a $d_{M_b} \times d_{M_b}$ real symmetric matrix. So $A = M = c^T c$ and $B = 0$.

Now $\mathrm{Tr}\, A = \mathrm{Tr}(c^T c) = \|c\|_F^2 = 1$ (normalization), and

$$\mathrm{Tr}(A^2) \;=\; \mathrm{Tr}((c^T c)^2) \;=\; \mathrm{Tr}(c^T c c^T c) \;=\; \mathrm{Tr}((cc^T)^2) \;=\; \mathrm{Tr}(\psi^2), \tag{82}$$

where $\psi = cc^\dagger = cc^T$ for real c. Thus $(\mathrm{Tr}\, A)^2 + 2\ \mathrm{Tr}(A^2) = 1 + 2\ \mathrm{Tr}(\psi^2)$.

EGH's (65) with real c gives $1 + \mathrm{Tr}(\psi^2) + \mathrm{Tr}(\psi\psi^T)$. For real symmetric ψ, $\psi^T = \psi$, so $\mathrm{Tr}(\psi\psi^T) = \mathrm{Tr}(\psi^2)$ and EGH's formula also equals $1 + 2\ \mathrm{Tr}(\psi^2)$.

The two match. □

A.4 Proof of (A.18′): generalized formula for V_β

A.4.1 Setup

Applied to the same bulk state, the map V_β (cloning β instead of α) produces:

$$\Psi_{m,i,n} \;=\; \sqrt{d_b}\, \psi_\alpha^m\, Q_{i,n}, \qquad Q_{i,n} \;\equiv\; b_n \sum_j c_{ij}\, u_{(n,j)}, \tag{83}$$

where now n is a free cloned-β index (not summed), and the structure $Q_{i,n} = b_n\, L_{i,n}$ factorizes with $L_{i,n} = \sum_j c_{ij}\, u_{(n,j)}$.

Tracing out α and the cloned β' yields

$$(\rho_{M_a})_{ik} \;=\; d_b \sum_n Q_{i,n}\,\overline{Q_{k,n}} \;=\; d_b\,(QQ^\dagger)_{ik}, \tag{84}$$

and

$$\mathrm{Tr}(\rho_{M_a}^2) \;=\; d_b^2\;\mathrm{Tr}\big((QQ^\dagger)^2\big) \;=\; d_b^2 \sum_{i,k,j,l} Q_{ij}\,\overline{Q_{kj}}\,Q_{kl}\,\overline{Q_{il}}. \tag{85}$$

(Here j, l index the cloned β dimension, not M_b.)

A.4.2 Expansion into components

Substituting $Q_{i,j} = b_j\,L_{i,j}$:

$$\mathrm{Tr}(\rho_{M_a}^2) \;=\; d_b^2 \sum_{i,j,k,l} |b_j|^2\,|b_l|^2\,L_{ij}\,\overline{L_{kj}}\,L_{kl}\,\overline{L_{il}}. \tag{86}$$

Each L is a linear function of u: $L_{i,j} = \sum_s c_{is}\,u_{(j,s)}$. The quartic product expands to

$$L_{ij}\,\overline{L_{kj}}\,L_{kl}\,\overline{L_{il}} \;=\; \sum_{s,t,u,v} c_{is}\,\overline{c_{kt}}\,c_{ku}\,\overline{c_{iv}}\,u_{(j,s)}\,u_{(j,t)}\,u_{(l,u)}\,u_{(l,v)}. \tag{87}$$

Applying Lemma A.2 to the fourth moment in u, with composite indices $a_1 = (j,s), a_2 = (j,t), a_3 = (l,u), a_4 = (l,v)$, yields three pair-matching contributions:

$$\mathrm{T}_1 \;=\; \delta_{a_1a_2}\delta_{a_3a_4} \;=\; \delta_{s,t}\,\delta_{u,v}, \tag{88}$$

$$\mathrm{T}_2 \;=\; \delta_{a_1a_3}\delta_{a_2a_4} \;=\; \delta_{j,l}\,\delta_{s,u}\,\delta_{t,v}, \tag{89}$$

$$\mathrm{T}_3 \;=\; \delta_{a_1a_4}\delta_{a_2a_3} \;=\; \delta_{j,l}\,\delta_{s,v}\,\delta_{t,u}. \tag{90}$$

Note that T_1 does *not* force $j = l$ while T_2 and T_3 do.

A.4.3 Evaluating the three contributions

Using $\psi = cc^\dagger$ (Hermitian, $\mathrm{Tr}\,\psi = 1$) and $\tilde{\psi} = cc^T$ (complex symmetric in general):

Contribution from $\mathbf{T}_1$ (general j, l):

$$\sum_{s,t,u,v} c_{is}\,\overline{c_{kt}}\,c_{ku}\,\overline{c_{iv}}\,\delta_{s,t}\delta_{u,v} \;=\; \Big(\sum_s c_{is}\,\overline{c_{ks}}\Big)\Big(\sum_u c_{ku}\,\overline{c_{iu}}\Big) \;=\; \psi_{ik}\,\psi_{ki} \;=\; |\psi_{ik}|^2. \tag{91}$$

Summed over i, k, j, l with weight $|b_j|^2|b_l|^2$:

$$\sum_{j,l}|b_j|^2|b_l|^2 \cdot \sum_{i,k}|\psi_{ik}|^2 \;=\; 1 \cdot 1 \cdot \mathrm{Tr}(\psi^2) \;=\; \mathrm{Tr}(\psi^2). \tag{92}$$

Contribution from $\mathbf{T}_2$ ($j = l$ enforced):

$$\sum_{s,t,u,v} c_{is}\,\overline{c_{kt}}\,c_{ku}\,\overline{c_{iv}}\,\delta_{s,u}\delta_{t,v} \;=\; \Big(\sum_s c_{is}\,c_{ks}\Big)\Big(\sum_t \overline{c_{kt}}\,\overline{c_{it}}\Big) \;=\; \tilde{\psi}_{ik}\,\overline{\tilde{\psi}_{ik}} \;=\; |\tilde{\psi}_{ik}|^2. \tag{93}$$

Summed with weight and $\delta_{j,l}$:

$$\sum_{j,l}|b_j|^2|b_l|^2\,\delta_{j,l} \cdot \sum_{i,k}|\tilde{\psi}_{ik}|^2 \;=\; \Big(\sum_j |b_j|^4\Big)\,\|\tilde{\psi}\|_F^2 \;=\; \mathrm{Tr}(p_\beta^2)\cdot\|\tilde{\psi}\|_F^2, \tag{94}$$

where $p_\beta \equiv \mathrm{diag}(|b_n|^2)$.

Contribution from $\mathbf{T}_3$ ($j = l$ enforced):

$$\sum_{s,t,u,v} c_{is}\,\overline{c_{kt}}\,c_{ku}\,\overline{c_{iv}}\,\delta_{s,v}\delta_{t,u} \;=\; \Big(\sum_{s} c_{is}\,\overline{c_{is}}\Big)\Big(\sum_{t}\overline{c_{kt}}\,c_{kt}\Big) \;=\; \psi_{ii}\,\psi_{kk}. \tag{95}$$

Summed:

$$\mathrm{Tr}(p_\beta^2)\cdot\Big(\sum_i \psi_{ii}\Big)\Big(\sum_k \psi_{kk}\Big) \;=\; \mathrm{Tr}(p_\beta^2)\cdot(\mathrm{Tr}\,\psi)^2 \;=\; \mathrm{Tr}(p_\beta^2), \tag{96}$$

using $\mathrm{Tr}\,\psi = 1$.

A.4.4 Assembly and identification

Collecting (85) with the factor $1/(d_b(d_b+2))$ from Lemma A.2:

$$\mathbb{E}_O\big[\mathrm{Tr}(\rho_{M_a}^2)\big] \;=\; \frac{d_b^2}{d_b(d_b+2)}\Big[\mathrm{Tr}(\psi^2)+\mathrm{Tr}(p_\beta^2)\big(\|\tilde\psi\|_F^2+1\big)\Big]. \tag{97}$$

It remains to identify $\|\tilde\psi\|_F^2$ with $\mathrm{Tr}(\rho\,\rho^{T_{M_b}})$.

Lemma A.4. *For ρ the density matrix on $\mathcal{H}_{M_a}\otimes\mathcal{H}_{M_b}$ with components $\rho_{(ij),(kl)} = c_{ij}\,\overline{c_{kl}}$, and $\rho^{T_{M_b}}$ its partial transpose on M_b,*

$$\mathrm{Tr}\big(\rho\,\rho^{T_{M_b}}\big) \;=\; \|\tilde\psi\|_F^2, \qquad \tilde\psi = cc^T. \tag{98}$$

Proof. The partial transpose has components $\rho^{T_{M_b}}_{(ij),(kl)} = \rho_{(il),(kj)} = c_{il}\,\overline{c_{kj}}$. Therefore

$$\mathrm{Tr}(\rho\,\rho^{T_{M_b}}) \;=\; \sum_{i,j,k,l}\rho_{(ij),(kl)}\,\rho^{T_{M_b}}_{(kl),(ij)} \;=\; \sum_{i,j,k,l} c_{ij}\,\overline{c_{kl}}\,c_{kj}\,\overline{c_{il}}. \tag{99}$$

Regroup:

$$= \sum_{i,k}\Big(\sum_j c_{ij}\,c_{kj}\Big)\Big(\sum_l \overline{c_{kl}}\,\overline{c_{il}}\Big) \;=\; \sum_{i,k}\tilde\psi_{ik}\,\overline{\tilde\psi_{ik}} \;=\; \|\tilde\psi\|_F^2. \tag{100}$$

□

Substituting into (97):

$$\boxed{\mathbb{E}_O\big[\mathrm{Tr}(\rho_{M_a}^2)\big]_{V_\beta|\psi_1\rangle} \;=\; \frac{d_b}{d_b+2}\Big[\mathrm{Tr}(\psi^2)+\mathrm{Tr}(p_\beta^2)\big(1+\mathrm{Tr}(\rho\,\rho^{T_{M_b}})\big)\Big],} \tag{101}$$

with $\psi = cc^\dagger$, $p_\beta = \mathrm{diag}(|b_n|^2)$, and ρ the bulk matter density matrix. □

A.4.5 Reduction to EGH (A.18)

For $|\psi_\beta\rangle = |0\rangle$, $p_\beta = \mathrm{diag}(1,0,\ldots,0)$ and $\mathrm{Tr}(p_\beta^2) = 1$. For real c, Lemma A.4's computation specializes using $\overline{c_{kl}} = c_{kl}$:

$$\mathrm{Tr}(\rho\,\rho^{T_{M_b}}) \;=\; \sum_{i,j,k,l} c_{ij}c_{kl}c_{kj}c_{il} \;=\; \sum_{i,k}(cc^T)_{ik}^2 \;=\; \mathrm{Tr}(\psi^2), \tag{102}$$

using $(cc^T)_{ik} = \sum_j c_{ij}c_{kj}$ is real symmetric and equal to ψ for real c. Substituting:

$$(101)\Big|_{\text{real } c,\ \psi_\beta=|0\rangle} \;=\; \frac{d_b}{d_b+2}\big[\mathrm{Tr}(\psi^2)+1\cdot(1+\mathrm{Tr}(\psi^2))\big] \;=\; \frac{d_b}{d_b+2}\big[1+2\ \mathrm{Tr}(\psi^2)\big]. \tag{103}$$

EGH (66) in the same limit: $\mathrm{Tr}(\omega^2) = \mathrm{Tr}(\omega\omega^T) = 1$ for $\omega = |0\rangle\langle 0|$, and $\mathrm{Tr}(\psi\psi^{T_{M_b}}) = \mathrm{Tr}(\psi^2)$ for real c (by the same Lemma A.4 computation). Thus EGH (66) also reduces to $\frac{d_b}{d_b+2}[1+2\ \mathrm{Tr}(\psi^2)]$.

The two match. □

A.5 Numerical verification

Both generalized formulas were verified against direct Monte Carlo simulation for complex bulk states. Six dimension configurations spanning $(d_\alpha, d_{M_a}, d_\beta, d_{M_b}) \in \{(2,2,2,2), (2,3,2,3), (3,3,3,3), (2,2,3,3)\}$ with both maximally-entangled and Haar-random c, at $N = 400$ samples of Haar-O per configuration.

Table 2: Verification of (81) for complex c, $|\psi_\beta\rangle$ Haar on $\mathcal{H}_\beta$. Columns show predicted vs. measured expected purity, SEM, and the z-score of the discrepancy.

$(d_\alpha, d_{M_a}, d_\beta, d_{M_b})$	state	prediction	measured	SEM	z
$(2,2,2,2)$	max-ent	1.1640	1.1484	0.018	-0.86
$(2,2,2,2)$	Haar	1.1515	1.1587	0.019	$+0.38$
$(2,3,2,3)$	max-ent	1.2237	1.2274	0.022	$+0.17$
$(3,3,3,3)$	max-ent	1.1015	1.0968	0.014	-0.33
$(3,3,3,3)$	Haar	1.5076	1.5104	0.048	$+0.06$
$(2,2,3,3)$	max-ent	1.4916	1.4814	0.046	-0.22

Pooled $\chi^2 = 1.08/6$ dof, well within expectation. No systematic trend in z values.

Table 3: Verification of (101), same configurations.

$(d_\alpha, d_{M_a}, d_\beta, d_{M_b})$	state	prediction	measured	SEM	z
$(2,2,2,2)$	max-ent	0.8378	0.8400	0.004	$+0.52$
$(2,2,2,2)$	Haar	1.2876	1.2916	0.029	$+0.14$
$(2,3,2,3)$	max-ent	1.0776	1.0593	0.019	-0.97
$(3,3,3,3)$	max-ent	0.6390	0.6400	0.003	$+0.31$
$(3,3,3,3)$	Haar	1.0262	1.0126	0.024	-0.56
$(2,2,3,3)$	max-ent	1.2334	1.2336	0.038	$+0.01$

Pooled $\chi^2 = 1.66/6$ dof, consistent with expectation.

In both cases, Monte Carlo verification of the original EGH formulas (65) and (66) at the *same* parameter configurations (but with real c and $|\psi_\beta\rangle = |0\rangle_\beta$) likewise passes pooled χ^2 tests, confirming that the generalizations specialize correctly.

Reproducibility is bit-identical across runs under the same seed.

A.6 Status

The generalizations (81) and (101) are minor but genuine extensions of EGH [3]'s published formulas, correcting for the implicit real-c and basis-state assumptions in the original derivations. They are not required for the main body of this paper — our two scaling theorems (Theorems 4.2 and 5.2) involve entirely different quantities — but they are included here because:

1. They were derived and verified in the course of calibrating EGH's result numerically (Phase 3 of our computational program), and that calibration was a prerequisite to the subsequent two-observer work;

2. They fill a real gap in the published EGH framework, specifically for bulk states with nonzero imaginary matter-factor amplitudes or non-basis-state β-pointers;

3. The proofs give a cleaner derivation than the full $O(n)$ Weingarten expansion would require, using only the fact that the first row of a Haar-random $O(d)$ matrix is uniform on the real sphere.

The formulas are proved rigorously above, reduce analytically to the EGH originals under the appropriate restrictions, and match direct Monte Carlo simulation to sub-σ precision in the general complex-bulk regime.

B Reproducibility

B.1 Software environment

All computations use the following package versions, pinned on a single Linux machine (Ubuntu 24.04 LTS, Python 3.12.3):

Package	Version	Use
`numpy`	2.4.4	linear algebra, random number generation
`scipy`	1.17.1	`unitary_group` (Haar unitaries), `ortho_group` (Haar orthogonals)
`pandas`	3.0.2	data tables and CSV I/O
`matplotlib`	3.10.8	figures
`mpmath`	1.3.0	exact evaluation of transcendental constants
`sympy`	1.14.0	analytic checkpoint computations
`statsmodels`	0.14.6	WLS and subleading-correction fits

Every `pip install` used `--break-system-packages` as required by Ubuntu 24 system Python; all results are reproducible under any equivalent install of the above versions.

B.2 Seed conventions

All Monte Carlo draws route through either `numpy.random.default_rng(seed)` or the project's `SeededRNG` wrapper (which threads a single `default_rng` through both numpy and `scipy.stats.unitary_group` for a unified stream):

```
class SeededRNG:
    def __init__(self, seed: int = 0xBADC0DE):
        self.rng = np.random.default_rng(int(seed))
    def haar_unitary(self, n):
        return unitary_group.rvs(n, random_state=self.rng)
    def haar_state(self, d):
        # complex Gaussian then normalize
        ...
    def aehpv_map(self, d_eff, d_fund):
        # first d_fund rows of haar_unitary(d_eff)
        ...
```

Each phase uses a distinct `BASE_SEED` constant, with per-point seeds derived deterministically from `BASE_SEED` and the relevant dimension parameters so that every data point's sample stream is fully determined by its nominal coordinates:

The seed-to-data correspondence is bit-identical across reruns under `numpy >= 2.0`: the same seed yields the same state vector, unitary, and statistics down to the last bit.

B.3 Sample sizes per data point

Phase 5 extended scan (Haar bulk)

Nine points with cumulative sample counts from merged batches:

Phase	BASE_SEED	Per-point seed formula
Phase 1 (HUZ/Colorado tables)	424242	`BASE + d_Ob*10000 + d_M*100 + d_fund`
Phase 2 (HUZ error scaling)	313131	`BASE + d_Ob*131 + d_M*11 + d_fund`
Phase 3 (EGH reproduction)	202020	`BASE + D_L*10000 + D_R*100 + D_C`
Phase 4 (two-observer setup)	414141	`BASE + d_OA*1000 + d_OB*100 + d_M*10 + d_fund`
Phase 5 (money plot)	505050	`BASE + d_B*10000 + batch_offset`
Phase 6 (state-class scan)	606060	`BASE + d_B*100 + class_code`
Phase 7 (theorem verification)	inline	`77700 + d_B` or similar per-script

d_B	N	notes
4	300	single batch
6	300	single batch
8	300	single batch
10	300	single batch
12	300	merged from $150 + 150$ with `phase5_boost_point.py`
14	200	merged from $100 + 100$
16	240	merged from $120 + 120$
20	190	merged from $100 + 90$
24	60	single batch (compute-bound at $d_{\text{eff}} = 2304$)

Batch-merge metadata preserved in `phase5_extended_scan.csv`. Batch offsets use independent seed streams (`BASE_SEED + d_B*10000 + batch_index`) to guarantee statistical independence across batches.

Phase 6 state-class scan

Haar and Product classes, six primary points plus Product extension:

d_B	Haar N	Product N
4	150	150
6	150	150
8	150	150
10	150	150
12	150	150
16	100	150
20	—	40 (out-of-sample extension)
24	—	20 (out-of-sample extension)

Phase 7 theorem verification

Per-figure sample sizes:

Figure 3 (Theorem 4.2, Product):

- Panel (a) Dirichlet variance: $N \in \{10^5, 10^5, 10^5, 10^5, 5 \cdot 10^4, 5 \cdot 10^4, 2.5 \cdot 10^4, 1.5 \cdot 10^4, 10^4\}$ for $d \in \{4, 8, 16, 32, 64, 128, 256, 512, 1024\}$.
- Panel (b) prefactor: $N \in \{10^5, 5 \cdot 10^4, 5 \cdot 10^4, 3 \cdot 10^4, 2.5 \cdot 10^4, 1.5 \cdot 10^4, 1.5 \cdot 10^4, 8 \cdot 10^3\}$.
- Panel (c) Gaussian ratio: same as (b).
- Panel (d) Phase-6 theory: $N = 30{,}000$ per theory point, paired with Phase 6 data.

Figure 4 (Theorem 5.2, Haar):

- Panels (a, b) large-d scan: $N \in \{10^5, 6 \cdot 10^4, 4 \cdot 10^4, 2 \cdot 10^4, 10^4, 4 \cdot 10^3\}$ for $d \in \{16, 24, 32, 48, 64, 96\}$ (234,000 samples total; seed stream $61000 + d$ matching `phase7_haar_subleading.py`).
- Panel (c) Phase-5 comparison: matched to Phase 5 N values above.
- Panel (d) out-of-sample: $d = 128$ at $N = 5{,}000$; $d_B = 18$ at $N = 60$ (full HUZ + V pipeline, cached in `phase7_dB18_ckpt.pkl`).

Structural identity verification (Figure 2)

Haar-V averages at $d_B \in \{4, 6, 8\}$ with $N_V \in \{500, 300, 200\}$ Haar-V draws per point, two bulk state classes. 18 diagonal entries compared per class (6 at $d_B = 4$, 6 at $d_B = 6$, 6 at $d_B = 8$).

B.4 Per-batch wall-time budget

The execution environment imposed a wall-time ceiling of approximately 5 minutes per bash invocation. This ruled out single-shot runs at large d_B (where per-sample cost scales as $d_{\text{eff}}^3 = (d_B^2 d_M)^3$ for the full two-observer HUZ + V simulation). Three workarounds enabled the large-d_B scan:

1. **Checkpoint-every-N-samples** (`phase5_boost_point.py`): pickle partial results to `phase5_cache/point_dB{N}.pkl` every 25–50 samples so a timeout at sample k loses at most 50 samples, not the full run.
2. **Independent batch seeds**: each invocation uses `BASE_SEED + d_B*10000 + batch_index` so running the same command twice extends the sample count rather than duplicating samples.
3. **Efficient two-observer entropy computation** (`two_observer_entropies_fast` in `phase5_money_plot.py`): replaces the naïve formation of the full joint density matrix (which would require ~ 270 GB at $d_B = 16$) with direct einsum contractions on the state tensor, reducing memory to ~ 2 MB at $d_B = 16$. Bit-identical to the naïve computation on five cross-checked test cases.

All Phase 5, 6, and 7 data was collected under these three mechanisms. A single fresh machine with no wall-time limits could reproduce the full scan in approximately 3–4 CPU-days on a single core.

B.5 File manifest

Full content of `/mnt/user-data/outputs/` relevant to the paper:

Phase 1 — HUZ and Colorado rules

- `phase1_rules_canonical.py` — unified backend, both rules, 8/8 gates
- `phase1_huz_table.csv` — 32 rows of HUZ-rule rank and entropy predictions
- `phase1_colorado_table.csv` — 24 rows of Colorado-rule predictions

Phase 2 — HUZ error scaling

- `phase2_huz_verification.py` — driver, three configs A/B/C, d_M scan
- `phase2_config_{A,B,C}.csv` — error-scaling tables per config
- `phase2_dM_scan.csv` — d_M dependence at fixed d_B
- `phase2_exponents.csv` — fitted exponents per config
- `phase2_analytic_check.py`, `.csv` — Weingarten prefactor verification

Phase 3 — EGH reproduction and generalized formulas

- `phase3_egh_reproduction.py` — AS^{2}R SWAP-test Page-formula reproduction
- `phase3_egh_as2r.csv` — 11 rows, three SWAP quantities
- `phase3_egh_direct.py` — direct EGH figure match + generalized formulas
- `phase3_egh_eq_4_{6,18}.csv` — EGH formulas verified on real c
- `phase3_generalized_4_{6,18}.csv` — generalized formulas verified on complex c (Appendix A, Tables 2–3)

Phase 4 — Two-observer HUZ setup

- `phase4_two_observers.py` — driver, gate checks, first scaling look
- `phase4_symmetric.csv`, `phase4_asymmetric.csv` — consistency gates
- `phase4_scan_dB.csv` — first 5-point scan at $d_B \in \{4, \ldots, 6\}$

Phase 5 — Money plot

- `phase5_money_plot.py` — canonical driver, includes `two_observer_entropies_fast`
- `phase5_boost_point.py` — checkpoint-per-batch extension driver
- `phase5_run_point.py` — single-point runner
- `phase5_extended_assemble.py` — merge batches into final scan
- `phase5_extended_scan.csv` — 9 points, total $N = 2190$ (final data for Figure 1 Haar curve)
- `phase5_subleading_fit.py`, `phase5_alt_subleading.py` — subleading ansatz fits
- `phase5_candidate_exponents.csv`, `phase5_extended_fit_summary.csv` — fit tables

Phase 6 — State-class dependence

- `phase6_state_class.py` — driver, both classes, per-point cached
- `phase6_scan.csv` — raw per-point means and SEMs
- `phase6_fits.csv` — pure and subleading fits per class

Phase 7 — Analytic verification

- `phase7_product_rigorous.py`, `phase7_dirichlet_rigor.py` — Theorem 4.2 levels (a, b, c)
- `phase7_rho_RA_verify.py`, `phase7_haar_rho_RA_verify.py` — structural identity (Figure 2)
- `phase7_theory_vs_phase6.py` + `phase7_theory_vs_phase6.csv` — Theorem 4.2 level (d)
- `phase7_haar_diagonal_theory.py`, `phase7_haar_asymptotic.py` — Theorem 5.2 levels (a, b)
- `phase7_haar_subleading.py` — subleading-correction fit (Theorem 5.2, §5.5)
- `phase7_haar_out_of_sample.py` — $d = 128$ no-V and $d_B = 18$ full-V out-of-sample tests
- `phase7_product_prediction.py`, `phase7_haar_prediction.py` — standalone theorem-prediction utilities

Paper figures

- `paper_figures_1.py` (v1) + `paper_figures_1v2.py` (final) — Figure 1 money plot
- `paper_figures_2.py` — Figure 2 structural identity
- `paper_figures_3.py` — Figure 3 Theorem 4.2 verification
- `paper_figures_4.py` — Figure 4 Theorem 5.2 verification
- `paper_figures_5.py` — Figure 5 combined landscape
- `fig{1..5}_*.{pdf,png}` — 300 dpi paper-quality figure files

B.6 Reproducibility verification

Every non-trivial data point has been spot-checked for bit-identical reproducibility: running the driver script a second time under the documented Python environment and seed yields identical CSV output to machine precision. This includes:

- Phase 1 rank predictions (integer equality, trivially reproducible)
- Phase 2 error-scaling measurements (float agreement to $\leq 10^{-12}$)
- Phase 3 EGH and generalized verifications (float agreement to $\leq 10^{-12}$)
- Phase 5 at $d_B \in \{4, 6, 8\}$ (float agreement within a single batch; merged-batch reproducibility verified to $\leq 10^{-10}$ after re-merging)
- Phase 6 at $d_B = 4$ (float agreement to $\leq 10^{-12}$)
- Phase 7 Lemma 4.1 Dirichlet variance at $d = 256$ (float agreement to $\leq 10^{-13}$)

The one caveat: merged-batch runs (Phase 5 at $d_B \geq 12$) are reproducible in aggregate but not strictly bit-identical across different orderings of batch execution, because numeric summation order affects the accumulated mean by $\leq 10^{-14}$. Individual batches are bit-identical.

B.7 Data and code availability

All Python source, CSV data, and figure files listed in §B.5 are included with this manuscript as supplementary material. The unified backend (`bh_lab_backend.py`, containing `SeededRNG`, `aehpv_map`, and the two-observer HUZ machinery) is available on request pending code release. A public archival deposit (Zenodo or equivalent) is planned at time of submission.

Acknowledgments and author contributions

The research program reported in this paper was conducted by the author in collaboration with Claude Opus 4.7 (Anthropic), acting as a computational and mathematical collaborator throughout. The author directed the research: set the overall question, chose which subquestions to pursue and which to defer, flagged errors and pressed on loose ends, decided when numerical evidence was sufficient to pause and when to push further, and was responsible for the final form of every claim in this paper. Claude performed the symbolic and numerical heavy lifting: it wrote and debugged the Monte Carlo code, carried out the Weingarten and Dirichlet-moment calculations, drafted prose against the author's specifications, and maintained the phase-by-phase research memos. Every theorem, equation, figure, and citation was reviewed by the author before inclusion.

The collaboration proceeded in a strict "PI-and-postdoc" structure: the author held the judgment and the agenda, Claude held the technical throughput. The paper's contribution stands on its mathematical and numerical merits, verified as documented in §7 and Appendix B, independently of the collaboration format. The collaboration format is disclosed here because the author believes openness about AI-assisted research is important as the practice becomes more common, and because the work would not have reached its current form without it.

All code, data, and reproducibility metadata are available as described in §B.7.

References

[1] Chris Akers, Netta Engelhardt, Daniel Harlow, Geoff Penington, and Shreya Vardhan. The black hole interior from non-isometric codes and complexity. *JHEP*, 06:155, 2024.

[2] Daniel Harlow, Mykhaylo Usatyuk, and Ying Zhao. Quantum mechanics and observers for gravity in a closed universe. *JHEP*, 02:108, 2026.

[3] Netta Engelhardt, Elliott Gesteau, and Daniel Harlow. Observer complementarity for black holes and holography. 2025. To appear.

[4] Stefano Antonini, Martí n Sasieta, and Brian Swingle. Cosmology from random entanglement. *JHEP*, 11:188, 2023.

[5] Stefano Antonini and Pratik Rath. Do holographic CFT states have unique semiclassical bulk duals? 2024.

[6] Kenneth Higginbotham. Helping observers in closed universes reach their full potential. *JHEP*, 03:183, 2026.

[7] Josh De Vuyst, Stefan Eccles, Philipp A. Hoehn, and Josh Kirklin. Crossed products and quantum reference frames: on the observer-dependence of gravitational entropy. *JHEP*, 07:063, 2025.

[8] Josh De Vuyst, Stefan Eccles, Philipp A. Hoehn, and Josh Kirklin. Gravitational entropy is observer-dependent. 2024.

[9] Chris Akers, Gracemarie Bueller, Oliver DeWolfe, Kenneth Higginbotham, Johannes Reinking, and Rudolph Rodriguez. On observers in holographic maps. *JHEP*, 05:201, 2025.

[10] Jonah Kudler-Flam and Edward Witten. Emergent Mixed States for Baby Universes and Black Holes. 2025.

[11] Takato Mori and Beni Yoshida. Baby universe as logical qubits: information recovery in random encoding. 2025.

[12] Zhi Li, Takato Mori, and Beni Yoshida. Tripartite Haar random state has no bipartite entanglement. 2025.

[13] Hong Liu. Towards a holographic description of closed universes. 2025.

[14] Hong Liu. "Filtering" CFTs at large N: Euclidean Wormholes, Closed Universes, and Black Hole Interiors. 2025.